J. Plasma Phys. (2026), *vol*. 92, E32 © The Author(s), 2026. Published by Cambridge University Press.
This is an Open Access article, distributed under the terms of the Creative Commons Attribution licence (https://creativecommons.org/licenses/by/4.0/), which permits unrestricted re-use, distribution and reproduction, provided the original article is properly cited. doi:10.1017/S0022377826101329

Collision operator for electron runaway in cold weakly ionised plasmas

Yeongsun Lee[1,2], Pavel Aleynikov[3], Peter de Vries[4], Jong-Kyu Park[1,5] and Yong-Su Na[1]

[1]Department of Nuclear Engineering, Seoul National University, Seoul, South Korea
[2]Nuclear Research Institute for Future Technology and Policy, Seoul National University, Seoul, South Korea
[3]Max-Planck Institute fur Plasmaphysik, Greifswald, Germany
[4]ITER Organization, Route de Vinon sur Verdon, CS 90 046, 13067 St Paul Lez Durance, France
[5]Princeton Plasma Physics Laboratory, Princeton, NJ 08543, USA

Corresponding author: Yong-Su Na, ysna@snu.ac.kr

(Received 6 September 2025; revision received 12 December 2025; accepted 9 January 2026)

In cold weakly ionised plasmas, the Dreicer generation mechanism can be non-diffusive as demonstrated in a recent study. By expanding the previous letter, we present the detailed description of a proper collision operator to precisely account for the non-diffusive electron kinetics. The operator appropriately combines the Fokker–Planck operator and Boltzmann operator where free-bound collision cross-sections are valid in the low-energy region. The proposed operator is envisaged to predict runaway electron generation in cold weakly ionised plasmas, particularly to design a runaway-free reactor tokamak start-up.

Key words: runaway electrons, fusion plasma

1. Introduction

In weakly ionised plasmas, inelastic collisions play key roles in runaway electron (RE) (Wilson 1925) generation by slowing down electrons (Gurevich 1961) and creating knock-on sources (Rosenbluth & Putvinski 1997). For highly energetic electrons, inelastic slowing down can be adequately described by the Fokker–Planck (FP) operator (Chandrasekhar 1943; Rosenbluth, MacDonald & Judd 1957) since the typical energy transfer is much smaller than their energy (Breizman *et al.* 2019). Similarly, free-bound knock-on collisions, often approximated as free–free knock-on under the assumption of negligible ionisation potential (McDevitt, Guo & Tang 2019), can be accounted for by the Boltzmann operator (Landau, Lifshitz & Pitaevskij 1981; Rosenbluth & Putvinski 1997). The main interest of previous studies on free-bound collision operators (Kirillov, Trubnikov & Trushin 1975; Mosher 1975; Hesslow *et al.* 2017, 2018; Breizman *et al.* 2019; Walkowiak *et al.* 2022; Savoye-Peysson *et al.* 2023) has concentrated on the dynamics of energetic electrons to comprehend undesirable disruption REs (Lehnen *et al.* 2008; Martín-Solís *et al.*

2017; Reux *et al.* 2021) due to the danger of triggering plasma instabilities (Snipes *et al.* 2008; Liu *et al.* 2023) and ability to damage the device (Nygren *et al.* 1997; Matthews *et al.* 2016; de Vries *et al.* 2023).

Start-up REs (Knoepfel & Zweben 1975; Knoepfel & Spong 1979; Sharma & Jayakumar 1988) are well highlighted recently for the upcoming ITER plasma initiation (de Vries & Gribov 2019; de Vries *et al.* 2023) since significant current carried by them complicates the start-up or even leads to failure (Gribov, Kavin & Lukash 2018; de Vries *et al.* 2020; Hoppe *et al.* 2022; Matsuyama *et al.* 2022; Lee *et al.* 2023*b*, 2024; de Vries *et al.* 2025). Yet, the collision models suitable for describing disruption REs may be inadequate for analysing start-up REs. For instance, the energy of start-up REs is insufficient to make use of the first-order Born-approximation (Landau & Lifshitz 2013) essential for the Bethe stopping power (Bethe 1930) and Thomas–Fermi models (Kirillov *et al.* 1975; Hesslow *et al.* 2017). That is, valid collision cross-sections are necessary for both elastic and inelastic collisions. In addition, energy transfer via inelastic collisions is predominantly hard when the incident electron energy is close to the ionisation potential. This necessitates individual inelastic collisions to be accounted for by the binary Boltzmann operator Landau & Lifshitz (2013). Furthermore, the background Maxwellian assumption needs to be verified under the strong effect of neutrals on electrons to adopt the linearised free–free collision operator (Helander & Sigmar 2005).

According to the classical Dreicer kinetics (Gurevich 1961; Connor & Hastie 1975), the key phase space region determining the formation of the Dreicer flow is the narrow singular layer across the critical momentum where the energy diffusion drives an upward flow. However, if the critical energy is close to the ionisation potential in cold weakly ionised plasmas, the key region can be wider from the minimum excitation energy to critical energy in which hard inelastic collisions should be considered by the binary Boltzmann operator. Indeed, it was recently elucidated that the binary nature of inelastic collisions allows quasi-frictionless acceleration for some particles and facilitates the Dreicer generation (Dreicer 1959), yielding significant enhancement in the generation rate (Lee *et al.* 2024). The collision operator aided by the correct cross-sections and Boltzmann operator was originally presented by Lee *et al.* (2024) to include this nature when designing a runaway-free reactor start-up scenario with better confidence, where plasma parameters remain far away from the RE generation parametric region. This paper expands on the collision operator by Lee *et al.* (2024) by (i) describing the model development for electron–hydrogen atom collisions in greater detail; (ii) explicitly verifying the background Maxwellian assumption in cold weakly ionised plasmas under the consideration of complete linearised Coulomb operator; and (iii) presenting the numerical method for implementation of this model into kinetic solvers using the finite volume method (FVM).

The paper is organised as follows. In § 2, we present the Fokker–Planck–Boltzmann (FPB) operator with appropriate free-bound collision cross-sections. In § 3, the numerical implementation of this operator will be clarified. In § 4, the operator is applied to solve the Dreicer problem.

2. Kinetic model

The kinetic equation for the electrons is

$$\frac{\partial f_e}{\partial t} + eE\left[\frac{\mu}{p^2}\frac{\partial}{\partial p}p^2 + \frac{1}{p}\frac{\partial}{\partial \mu}\left(1-\mu^2\right)\right] f_e = C\{f_e\}, \tag{2.1}$$

https://doi.org/10.1017/S0022377826101329 Published online by Cambridge University Press

where $f_e(p, \mu)$ is the electron distribution function, p is particle momentum and $\mu = \cos\theta$ is the cosine of pitch-angle θ. Suppose the pure weakly ionised plasmas and assume hydrogen is in the ground state. There are two types of interactions depending on colliding species. Charged particles interact with each other through the long-range Coulomb interaction. The FP operator appropriately describes such inverse-square forces (Rosenbluth *et al.* 1957); the free–free knock-on collisions (Rosenbluth *et al.* 1957; Chiu *et al.* 1998) are negligible due to low ionisation fraction. However, the interaction between an electron and a hydrogen atom is short-range (close) due to the screened charge. We apply the FPB operator to account for electron–hydrogen atom interactions,

$$\mathcal{C}\{f_e\} = \mathcal{C}^{eH}\{f_e\} + \mathcal{C}_{FP}\{f_e\}, \tag{2.2}$$

where $\mathcal{C}^{eH}\{f_e\}$ is the FPB operator for electron–H atom interactions and $\mathcal{C}_{FP}\{f_e\}$ is the FP operator for collisions with charged particles. The FPB operator consists of two parts:

$$\mathcal{C}^{eH}\{f_e\} = \mathcal{C}^{soft}_{FP}\{f_e\} + \mathcal{B}^{hard}\{f_e\}, \tag{2.3}$$

where $\mathcal{C}^{soft}_{FP}\{f_e\}$ is the FP operator that includes all elastic collisions and soft inelastic collisions, and $\mathcal{B}^{hard}\{f_e\} = \mathcal{B}^{hard}_{iz}\{f_e\} + \mathcal{B}^{hard}_{ex}\{f_e\}$ is the Boltzmann operator accounting only for hard inelastic collisions. The subscripts iz and ex denote ionising and exciting collisions, respectively. In $\mathcal{C}^{soft}_{FP}\{f_e\}$, the integral boundary of the Coulomb logarithm is appropriately selected to avoid the double counting of collisions (Embréus *et al.* 2018).

An inelastic collision is soft if the accompanied energy loss is sufficiently small compared with the incident electron energy and otherwise hard. We introduce the soft–hard separation factor h for the systematic categorisation. If the energy loss ratio of the incident electron is higher than h, such collisions are hard and included in $\mathcal{B}^{hard}\{f_e\}$; otherwise, any excitation or ionisation collision is described by $\mathcal{C}^{soft}_{FP}\{f_e\}$.

Let T be the kinetic energy of the incident electron, W be that of the ejected electron, $T - W$ be that of the scattered electron and lowercase representation (t, w and $t - w$) indicate normalisation by the binding energy of the ejected electron B. We adopt the convention to call the fast one scattered and the slower one ejected after ionising collisions due to the indistinguishability of electrons, i.e. interchanging interpretation of W and $T - W$ if $W > T - W$. That is, the energy loss of the incident electron is $W + B$ when $T - W > W$, but is $T - W$ when $T - W < W$. Inelastic collisions are categorised by the corresponding energy loss ratio $\min\{(1 + w), (t - w)\}/t$ under this convention,

$$\text{Collision is hard if } \frac{\min\{(1 + w), (t - w)\}}{t} > h, \tag{2.4}$$

$$\text{Collision is soft if } \frac{\min\{(1 + w), (t - w)\}}{t} < h. \tag{2.5}$$

The scattered and ejected electron are regarded as the test and field particle in kinetic treatment.

This section is organised as follows. To clarify the calculation procedure and provide a convenient normalised form, we first derive $\mathcal{B}^{hard}$ and $\mathcal{C}^{soft}_{FP}$ in SI units in §§ 2.1 and 2.2, respectively, and then normalise them at the end of each section. In § 2.3, invariance in h is proven. Section 2.4 is about $\mathcal{C}_{FP}$. Electron acceleration mechanism is discussed in § 2.5.

https://doi.org/10.1017/S0022377826101329 Published online by Cambridge University Press

2.1. *Boltzmann collision model*

2.1.1. Hard ionising collisions

Inelastic collisions accounted for by the Boltzmann operator require the differential cross-section, which informs the distribution of the ejected electrons. We apply the RBED model (Kim, Santos & Parente 2000), which is the relativistic extension of the binary-encounter-dipole (BED) model (Kim & Rudd 1994). Note that the BED model successfully reproduced the experimentally measured total ionisation cross-section (Kim & Rudd 1994). In addition, the energy distribution of secondary (ejected) electrons of the BED model has a good agreement with that of experimental data (Kim & Rudd 1994). Therefore, this model is appropriate to use for our purpose.

The singly differential cross-section (SDCS) of the RBED model (Kim *et al.* 2000) is

$$\frac{\partial\sigma_{iz}(W,T)}{\partial W}=\frac{4\pi a_0^2\alpha_{fs}^4 N}{(\beta_t^2+\beta_u^2+\beta_b^2)2b'}\left\{\frac{(N_i/N)-2}{t+1}\left(\frac{1}{w+1}+\frac{1}{t-w}\right)\frac{1+2t'}{(1+t'/2)^2}\right.$$
$$+[2-(N_i/N)]\left[\frac{1}{(w+1)^2}+\frac{1}{(t-w)^2}+\frac{b'^2}{(1+t'/2)^2}\right]$$
$$\left.+\frac{1}{N(w+1)}\frac{\mathrm{d}f(w)}{\mathrm{d}w}\left[\ln\left(\frac{\beta_t^2}{1-\beta_t^2}\right)-\beta_t^2-\ln(2b')\right]\right\}, \tag{2.6}$$

where the prime indicates normalisation by the rest energy of an electron mc^2 (not B), e.g. $t'=T/mc^2$, β_A is the associated normalised relativistic velocity with energy $A\in(t,b,u)$ (i.e. $\beta_t^2=1-1/(1+t')^2$, $\beta_b^2=1-1/(1+b')^2$ and $\beta_u^2=1-1/(1+u')^2$), U is the average orbital kinetic energy of the target electron, a_0 is the Bohr radius, α_{fs} is the fine-structure constant, N is the orbital electron occupation number, $\mathrm{d}f(w)/\mathrm{d}w$ is the differential oscillator strength and $N_i\equiv\int_0^\infty \mathrm{d}f/(\mathrm{d}w)\,\mathrm{d}w$. This model was developed by combining the Mott cross-section (Mott 1930) and Bethe cross-section (Bethe 1930). The Bethe cross-section accounts for the dipole contribution, the last line in (2.6) proportional to $1/(w+1)\,\mathrm{d}f(w)/(\mathrm{d}w)$, which is unfortunately not symmetric under interchanging two electrons after the collision. Due to the indistinguishability of electrons, we only use the ejected-electron part of (2.6) including description of the scattered-electron part, i.e. $(\partial\sigma_{iz})/(\partial W)(W,T)=(\partial\sigma_{iz})/(\partial W)(T-W-B,T)$ if $W>(T-B)/2$.

The number of hard ionising collisions by incident electrons with $\boldsymbol{p}_1$ that produces electrons with $\boldsymbol{p}$ in phase space volume $\mathrm{d}^3\boldsymbol{p}_1\,\mathrm{d}^3\boldsymbol{p}$ during $\mathrm{d}t$ is

$$(\mathrm{d}n)_{iz}^{hard}\,\mathrm{d}\boldsymbol{p}_1\,\mathrm{d}\boldsymbol{p}=\mathcal{H}(p_1-p_{bnd})f_e(\boldsymbol{p}_1)\mathrm{d}\boldsymbol{p}_1\left[\frac{\partial\sigma(T,W)}{\partial W}f_{\tilde{\mu}}(\boldsymbol{p}_1,\boldsymbol{p})\,\mathrm{d}W\,\mathrm{d}\mu\,\mathrm{d}\phi\right]v_1 n_H\,\mathrm{d}t, \tag{2.7}$$

where n_H is hydrogen density and $f_{\tilde{\mu}}(\boldsymbol{p}_1,\boldsymbol{p})$ is the scattering angle distribution. Because the SDCS does not contain $f_{\tilde{\mu}}(\boldsymbol{p}_1,\boldsymbol{p})$, we impose low- and high-energy asymptotes on $f_{\tilde{\mu}}(\boldsymbol{p}_1,\boldsymbol{p})$. When the electron energy is low, the pitch-angle scattering is strong. In addition, the free-bound hard collisions by energetic electrons can be approximated as the free–free knock-on collisions (Møller 1932; Breizman *et al.* 2019). Therefore, we prescribe $f_{\tilde{\mu}}(\boldsymbol{p}_1,\boldsymbol{p})$ by interpolating the isotropic and Moller

https://doi.org/10.1017/S0022377826101329 Published online by Cambridge University Press

scattering angle distribution (Møller 1932),

$$f_{\tilde{\mu}}(\boldsymbol{p}_1, \boldsymbol{p}) = \frac{1/2 + (\delta(\tilde{\mu} - \mu^*) - 1/2)\mathcal{S}(\ln(p/0.1mc))}{2\pi}, \tag{2.8}$$

where $\mu^* = \sqrt{(\gamma_1 + 1)(\gamma - 1)/(\gamma_1 - 1)(\gamma + 1)}$ is the cosine of the Moller scattering angle, $\tilde{\mu} = (\boldsymbol{p}_1 \cdot \boldsymbol{p})/(p_1 p)$ is cosine of deflection angle, δ is the Dirac-delta function and $\mathcal{S}(x) \equiv 1/(1 + e^{-x})$ is the sigmoid function. Under $\mathcal{S}$, $f_{\tilde{\mu}}(\boldsymbol{p}_1, \boldsymbol{p})$ approaches the relativistic limit $(\delta(\tilde{\mu} - \mu^*)/2\pi)$ as p exceeds 0.1. Note (2.8) satisfies $\int \mathrm{d}\mu\, \mathrm{d}\phi f_{\tilde{\mu}}(\boldsymbol{p}_1, \boldsymbol{p}) = 1$.

The produced electrons include the test particles that remain after losing the energy through the hard ionising collisions and the field particles created by all ionising collisions. When $t > 2w + 1$ is met, the produced electrons are the field particles. The associated momentum $mc\sqrt{(2w' + b' + 1)^2 - 1}$ is the minimum value of p_1. In addition, there is no ionising collision if $t < w + 1$. In this case, the corresponding momentum $mc\sqrt{(w' + b' + 1)^2 - 1}$ is the maximum of p_1. Furthermore, the hard collision condition demands $t > w/(1 - h)$, i.e. $p_1 > mc\sqrt{(w'/(1 - h) + 1)^2 - 1}$. The three constraints for p_1 yield the lower boundary for hard ionising collisions,

$$p_{bnd} = mc\left\{ \min_2 \left(\sqrt{(w' + b' + 1)^2 - 1}, \sqrt{\left(\frac{w'}{1 - h} + 1\right)^2 - 1}, \sqrt{(2w' + b' + 1)^2 - 1} \right) \right\}, \tag{2.9}$$

where

$$\min_2(a, b, c) \equiv \min(a, \max(b, c)) \tag{2.10}$$

is the second minimum function.

The Boltzmann operator can be obtained by taking an integral $\int \mathrm{d}\boldsymbol{p}_1$ and dividing by $\mathrm{d}t\, \mathrm{d}\boldsymbol{p}$,

$$\mathcal{B}_{iz}^{hard}\{f_e\} = \frac{\int_{p_1}\left[(\mathrm{d}n)_{iz}^{hard}\, \mathrm{d}\boldsymbol{p}_1 \mathrm{d}\boldsymbol{p}\right]}{\mathrm{d}t\, \mathrm{d}\boldsymbol{p}} - \frac{\int_{p_1}\left[(\mathrm{d}n)_{iz}^{hard}\, \mathrm{d}\boldsymbol{p}_1\, \mathrm{d}\boldsymbol{p}\right](\boldsymbol{p} \leftrightarrow \boldsymbol{p}_1)}{\mathrm{d}t\, \mathrm{d}\boldsymbol{p}}, \tag{2.11}$$

where $(\boldsymbol{p} \leftrightarrow \boldsymbol{p}_1)$ is the interchange operator of $\boldsymbol{p}$ and $\boldsymbol{p}_1$. This can be rewritten as

$$\mathcal{B}_{iz}^{hard}\{f_e\} = n_H \frac{v}{p^2} \int_{p_1 \geqslant p_{pnd}} \mathrm{d}\boldsymbol{p}_1 \left[f_e(\boldsymbol{p}_1) v_1 \frac{\partial \sigma_{iz}(W, T)}{\partial W} f_{\tilde{\mu}}(\boldsymbol{p}_1, \boldsymbol{p}) \right] - \nu_{iz}^{hard} f_e(\boldsymbol{p}), \tag{2.12}$$

where, $\mathrm{d}W/\mathrm{d}p = v$ is used, $\nu_{iz}^{hard} = n_H v \sigma_{iz}^{hard}(T)$ is the hard ionising collision frequency with the total cross section of hard ionising collisions $\sigma_{iz}^{hard}(T)$

$$\sigma_{iz}^{hard}(T) = B \int_{w_{bnd}}^{(t-1)/2} \mathrm{d}w \frac{\partial \sigma_{iz}(W, T)}{\partial W}. \tag{2.13}$$

Estimating the total cross-section has the upper boundary given by $(t - 1)/2$ because collisions are doubly counted above this. Moreover, there is no ionising collision for $w < 0$. The hard collision condition yields $w > ht - 1$ provided that w is of the ejected particle between 0 and $(t - 1)/2$; the residual part of the w-region

https://doi.org/10.1017/S0022377826101329 Published online by Cambridge University Press

from 0 to $ht-1$ corresponds to soft ionising collisions and thereby is covered by the FP operator. The resulting integral boundary w_{bnd} is

$$w_{bnd} = \min_2\left(0, ht-1, \frac{t-1}{2}\right). \tag{2.14}$$

After multiplying by p^2, we take an integral $\int \mathrm{d}\phi$ and represent $\mathcal{B}_{iz}$ using $F_e(p,\mu) = \int \mathrm{d}\phi p^2 f_e(\boldsymbol{p})$,

$$\begin{aligned} 2\pi p^2 \mathcal{B}_{iz}^{hard}\{f_e\} = n_H v \int_{p_{bnd}} \mathrm{d}p_1 \int_{-1}^{1} \mathrm{d}\mu_1 \left[F_e(p_1,\mu_1) v_1 \frac{\partial \sigma_{RBED}(W,T)}{\partial W} \right] \\ \times \left(\frac{1}{2} + \left(\frac{\mathcal{H}((1-\mu^2)(1-\mu_1^2) - (\mu^* - \mu\mu_1)^2)}{\pi\sqrt{(1-\mu^2)(1-\mu_1^2) - (\mu^* - \mu\mu_1)^2}} - \frac{1}{2} \right) \mathcal{S}(\ln(p/0.1mc))) \right) \\ - \nu_{iz}^{hard} F_e(p,\mu) \end{aligned} \tag{2.15}$$

with the help of the gyro-phase averaged Moller scattering angle (Aleynikov *et al.* 2014; Boozer 2015; Breizman *et al.* 2019)

$$\int \mathrm{d}\phi \delta(\tilde{\mu} - \mu^*) = \frac{2\mathcal{H}((1-\mu^2)(1-\mu_1^2) - (\mu^* - \mu\mu_1)^2)}{\sqrt{(1-\mu^2)(1-\mu_1^2) - (\mu^* - \mu\mu_1)^2}}. \tag{2.16}$$

2.1.2. Hard exciting collisions

Hard exciting collisions are considered using the asymptotic expression of excitation cross-section (Stone, Kim & Desclaux 2002). This follows the BE-scaled plane wave Born (PWB) cross-sections (Kim 2001), which have a good agreement with the convergent close coupling (CCC) model (Kim 2001). The non-relativistic expression valid up to nearly 10 keV is appropriate for computing the runaway creation rate in the weakly ionised plasmas due to the low critical energy for runaway condition. The BE-scaled PWB cross-section does not include resonance effects (Stone *et al.* 2002). However, the error only exists in the limited region of phase space, i.e. at the near-threshold energy, and thus does not influence the electron acceleration significantly. Only the $1s \to np$ transitions are considered since they are more likely than $1s \to ns$; the former is optically allowed, whereas the latter is optically forbidden (see § 3.2 of Inokuti 1971).

The asymptotic cross-section of electron impact excitation accompanying the $1s \to np$ transition has a form

$$\sigma_{asympt}^{1s\to np}(T) = \frac{4\pi a_0^2 R}{T + B + E_{1n}}[a_{1n}\ln(T/R) + b_{1n} + c_{1n}R/T], \tag{2.17}$$

where a_{1n}, b_{1n} and c_{1n} are coefficients of the asymptotic expression found in table 1 of Stone *et al.* (2002), E_{1n} is the excitation energy for the $1s \to np$ transition and R is the Rydberg energy. The symbol of $\sigma_{asympt}^{1s\to np}(T)$ is replaced by $\sigma_{ex}^{1n}(T)$ in the following for brevity. The energy space region of incident electron to participate in hard exciting collisions is limited as $E_{1n} \leqslant T \leqslant E_{1n}/h$ due to the fixed excitation energy, where the upper bound ensures that the collisions are hard, i.e. $h \leqslant T/E_{1n}$. Hence, the scattering angle distribution is presumed as isotropic. The number of

https://doi.org/10.1017/S0022377826101329 Published online by Cambridge University Press

hard exciting collisions involving electron momentum transition from $\boldsymbol{p}_1$ to $\boldsymbol{p}$ in phase space volume $\mathrm{d}\boldsymbol{p}_1\,\mathrm{d}\boldsymbol{p}$ during $\mathrm{d}t$ is

$$(\mathrm{d}n)^{hard}_{ex,1s\to np}\mathrm{d}\boldsymbol{p}_1\,\mathrm{d}\boldsymbol{p} = f_e(\boldsymbol{p}_1)\,\mathrm{d}\boldsymbol{p}_1\left[\frac{\sigma^{1n}_{ex}(T)}{4\pi}\delta(T-W-E_{1n})\,\mathrm{d}W\,\mathrm{d}\mu\,\mathrm{d}\phi\right]v_1 n_H\,\mathrm{d}t. \tag{2.18}$$

The Boltzmann operator can be obtained by

$$\mathcal{B}^{hard}_{ex,1s\to np}\{f_e\} = \frac{\int_{\boldsymbol{p}_1}\left[(\mathrm{d}n)^{hard}_{ex,1s\to np}\,\mathrm{d}\boldsymbol{p}_1\,\mathrm{d}\boldsymbol{p}\right]}{\mathrm{d}t\,\mathrm{d}\boldsymbol{p}} - \frac{\int_{\boldsymbol{p}_1}\left[(\mathrm{d}n)^{hard}_{ex,1s\to np}\,\mathrm{d}\boldsymbol{p}_1\,\mathrm{d}\boldsymbol{p}\right](\boldsymbol{p}\leftrightarrow\boldsymbol{p}_1)}{\mathrm{d}t\,\mathrm{d}\boldsymbol{p}}. \tag{2.19}$$

This can be rewritten as

$$\mathcal{B}^{hard}_{ex,1s\to np}\{f_e\} = \frac{\nu^{hard}_{ex,1s\to np}(p^+)F^0_e(p^+)}{4\pi p^2}\frac{v(p)}{v(p^+)} - \nu^{hard}_{ex,1s\to np}(p)f_e(\boldsymbol{p}), \tag{2.20}$$

where $F^0_e = \int \mathrm{d}\mu F(p,\mu)$, $p^+ = mc\sqrt{(T'+E'_{1n}+1)^2-1}$, $\nu^{hard}_{ex,1s\to np}$ is the hard exciting collision frequency due to the $1s\to np$ transition. Here, $\nu^{hard}_{ex,1s\to np}$ depends on its argument; for example, $\nu^{hard}_{ex,1s\to np}(p^+_{1n}) = n_H v(p^+_{1n})\sigma^{1n}_{ex}(T+E_{1n})\mathcal{H}(E_{1n}/(T+E_{1n})-h)$ and $\nu^{hard}_{ex,1s\to np}(p) = n_H v(p)\sigma^{1n}_{ex}(T)\mathcal{H}(E_{1n}/T-h)$.

Multiplying by p^2, we take an integral $\int \mathrm{d}\phi$, and represent $\mathcal{B}^{hard}_{ex,1s\to np}\{f_e\} = \mathcal{B}^{hard,+}_{ex,1s\to np}\{f_e\} - \mathcal{B}^{hard,-}_{ex,1s\to np}\{f_e\}$:

$$2\pi p^2\mathcal{B}^{hard}_{ex,1s\to np}\{f_e\} = \frac{\nu^{hard}_{ex,1s\to np}(p^+_{1n})}{2}\frac{v(p)}{v(p^+_{1n})}F^0_e(p^+_{1n}) - \nu^{hard}_{ex,1s\to np}(p)F_e(p,\mu). \tag{2.21}$$

We consider hard exciting collisions up to the $1s\to 10p$ transition, i.e.

$$2\pi p^2\mathcal{B}^{hard}_{ex}\{f_e\} = \sum_{n=2}^{10} 2\pi p^2\mathcal{B}^{hard}_{ex,1s\to np}\{f_e\}. \tag{2.22}$$

2.1.3. Normalisation

Let $\tilde{p} = p/mc$, $\tilde{t} = t/\tau_c$, $\tilde{\nu}^{hard}_{iz} = \nu^{hard}_{iz}\tau_c$ and $\tilde{\nu}^{hard}_{ex} = \nu^{hard}_{ex}\tau_c$, where $\tau_c \equiv (4\pi\varepsilon_0^2 m_e^2 c^3)/(e^4 n_e ln\Lambda)$. Neglecting tilde, $2\pi p^2\mathcal{B}^{hard}\{f_e\}$ becomes

$$\begin{aligned}2\pi p^2\mathcal{B}^{hard}\{f_e\} = {} & n_H mc^3\tau_c\frac{p}{\gamma}\left[\int_{p_{bnd}}\mathrm{d}p_1\mathrm{d}\mu_1\frac{\mathrm{d}\sigma_{iz}}{\mathrm{d}W}\right.\\ & \times\left(\left(\frac{\mathcal{H}((1-\mu^2)(1-\mu_1^2)-(\mu^*-\mu\mu_1)^2)}{\pi\sqrt{(1-\mu^2)(1-\mu_1^2)-(\mu^*-\mu\mu_1)^2}}-\frac{1}{2}\right)\frac{1}{1+\frac{0.1}{p}}+\frac{1}{2}\right)\frac{p_1}{\gamma_1}F_e(p_1,\mu_1)\Bigg]\\ & -\nu^{hard}_{iz}F_e(p,\mu)+\sum_{n=2}^{10}\left[\frac{\nu^{hard}_{ex,1s\to np}(p^+_{1n})}{2}\frac{\beta(p)}{\beta(p^+_{1n})}F^0_e(p^+_{1n})-\nu^{hard}_{ex,1s\to np}(p)F_e(p,\mu)\right].\end{aligned} \tag{2.23}$$

https://doi.org/10.1017/S0022377826101329 Published online by Cambridge University Press

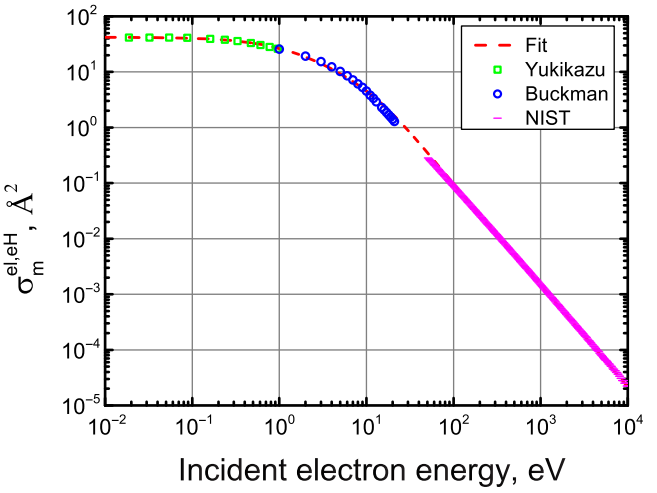


FIGURE 1. Momentum transfer cross-section from the refined model with χ (red dashed curve); Itikawa (1974) (green square marker); Buckman & Elford (2000) (blue circle marker); and NIST standard database (Jablonski, Salvat & Powell 2004; Salvat, Jablonski & Powell 2005) (magenta bar).

2.2. *Fokker–Planck collisional model*

2.2.1. Elastic collisions

To account for elastic scattering of low energy electrons due to collision with hydrogen neutrals, we borrow a function form from the Thomas–Fermi (TF) model (Breizman *et al.* 2019) and refine it by fitting against experimental data (Itikawa 1974; Buckman & Elford 2000; Jablonski *et al.* 2004; Salvat *et al.* 2005). The direct usage of the TF model is not rigorous because the TF model is valid for the partial screening effect of high-Z partially stripped ions/neutrals on energetic electrons: the majority of bound electrons need to have large principal quantum numbers and an incident electron should be energetic due to the first-order Born approximation (Landau & Lifshitz 2013; Hesslow *et al.* 2018).

According to Zhogolev & Konovalov (2014) and Breizman *et al.* (2019), the function form of the elastic collision frequency is known as

$$\nu_{el} = n_H c \frac{e^4}{4\pi\varepsilon_0^2 m^2 c^4} I_2(y), \tag{2.24}$$

where $I_2(y)$ is the second screening coefficient with $y = 274p/mc$. This coefficient grows logarithmically with y at the high-energy region, i.e. $I_2(y) \approx I_2(y_*) + \ln(y/y_*)$ with $y_* = 26$. We extrapolate this to the low-energy region, ensuring that I_2 approaches 0,

$$I_2(y) \approx I_2(y_*) + \frac{\ln\left[(y/y_*)^4 + \exp(-I_2(y_*))^4\right]}{4}. \tag{2.25}$$

Let $\nu_{el}^{ref} \equiv \chi \nu_{el}$ be the refined frequency with a correction factor χ. The outcome of refinement is displayed in figure 1 by fitting the momentum transfer (transport) cross-section $\sigma_m^{el,eH} \approx \chi(e^4)/(4\pi\varepsilon_0^2 m_e^2 v^4) I_2$ to those of experimental data (Itikawa 1974; Buckman & Elford 2000) and the NIST Standard Database (Jablonski *et al.* 2004; Salvat *et al.* 2005). The red curve goes to the magenta bars for high-energy

https://doi.org/10.1017/S0022377826101329 Published online by Cambridge University Press

particles while aligning well with experimental data at low energy range. In fact, R^2 score is approximately 0.999. The fitting finds

$$\chi = 1 + \frac{a^{el}(511\,000(\gamma-1))^{b^{el}}}{1 + c^{el}(511\,000(\gamma-1))^{b^{el}}}, \tag{2.26}$$

where $a^{el} = 79.837201$, $b^{el} = -1.0992754$ and $c^{el} = 1.6387662$.

2.2.2. Soft ionising collisions

Let the stopping power of soft ionising collisions on electrons have the logarithmic factor

$$\left(\frac{\mathrm{d}\mathcal{E}}{\mathrm{d}t}\right)_{iz}^{soft} = -\frac{n_H e^4}{4\pi\varepsilon_0^2 m v}\ln\Lambda_{iz}^{soft}. \tag{2.27}$$

The stopping cross-section $\sigma_{iz}^{sti,soft}(T)$ also measures the net effect of soft ionising collisions on energy loss,

$$\sigma_{iz}^{sti,soft}(T) = \int_0^{W_{bnd}} (B+W)\frac{\mathrm{d}\sigma_{iz}(W,T)}{\mathrm{d}W}\,\mathrm{d}W, \tag{2.28}$$

where $W_{bnd} = B w_{bnd}$. After straightforward calculation, for $w_{bnd} = ht - 1$,

$$\begin{aligned}\sigma_{iz}^{sti,soft}(T) = \frac{4\pi a_0^2\alpha_{fs}^4 N}{(\beta_t^2+\beta_u^2+\beta_b^2)2b'}\Bigg\{&(f(ht-1)-f(0))\left[\ln\left(\frac{\beta_t^2}{1-\beta_t^2}\right)-\beta_t^2-\ln(2b')\right]\\ &+\left(2-\frac{N_i}{N}\right)\left[\frac{ht}{1+(1-h)t}-\frac{1}{t}+\ln\frac{1+(1-h)t}{t}\frac{1+2t'}{(1+t'/2)^2}+\ln ht\right.\\ &\left.+\ln\frac{1+(1-h)t}{t}+\frac{b'^2}{(1+t'/2)^2}\frac{h^2t^2-1}{2}\right]\Bigg\},\end{aligned} \tag{2.29}$$

for $w_{bnd} = (t-1)/2$,

$$\begin{aligned}\sigma_{iz}^{sti,soft}(T) = \frac{4\pi a_0^2\alpha_{fs}^4 N}{(\beta_t^2+\beta_u^2+\beta_b^2)2b'}\Bigg\{&\left(f\left(\frac{t-1}{2}\right)-f(0)\right)\left[\ln\left(\frac{\beta_t^2}{1-\beta_t^2}\right)-\beta_t^2-\ln(2b')\right]\\ &+\left(2-\frac{N_i}{N}\right)\left[1-\frac{1}{t}+\ln\frac{t+1}{2t}\frac{1+2t'}{(1+t'/2)^2}+2\ln\frac{t+1}{2}\right.\\ &\left.-\ln t+\frac{b'^2}{(1+t'/2)^2}\frac{t^2+2t-3}{8}\right]\Bigg\},\end{aligned} \tag{2.30}$$

and for $w_{bnd} = 0$,

$$\sigma_{iz}^{sti,soft}(T) = 0, \tag{2.31}$$

https://doi.org/10.1017/S0022377826101329 Published online by Cambridge University Press

where $f(w) = \int \mathrm{d}f/\mathrm{d}w(w)\,\mathrm{d}w = -b/(1+w) - c/(2(1+w)^2) - d/(3(1+w)^3) - e/(4(1+w)^4)$ with $b = -2.2473 \times 10^{-2}$, $c = 1.1775$, $d = -4.6264 \times 10^{-1}$ and $e = 8.9064 \times 10^{-2}$ listed in table I of Kim & Rudd (1994).

The stopping power estimated from $\sigma_{iz}^{sti,soft}(T)$ is

$$\left(\frac{\mathrm{d}\mathcal{E}}{\mathrm{d}t}\right)_{iz}^{soft} = -n_H v \sigma_{iz}^{sti,soft} \equiv -\nu_{iz}^{sti,soft}. \tag{2.32}$$

Equating (2.27) and (2.32) yields

$$\ln \Lambda_{iz}^{soft} = \frac{4\pi\varepsilon_0^2 m v}{n_H e^4} \nu_{iz}^{sti,soft}. \tag{2.33}$$

2.2.3. Soft exciting collisions

Let the stopping power of soft exciting collisions on electrons have the logarithmic factor

$$\left(\frac{\mathrm{d}\mathcal{E}}{\mathrm{d}t}\right)_{ex}^{soft} = -\frac{n_H e^4}{4\pi\varepsilon_0^2 m v} \ln \Lambda_{ex}^{soft}. \tag{2.34}$$

The stopping cross-section of soft exciting collision is $\sigma_{ex}^{ste,soft} = \sum_{n=2,10} \sigma_{ex}^{1n} E_{1n} \mathcal{H}(T - (E_{1n}/h))$ due to fixed excitation energy. The stopping power estimated from $\sigma_{ex}^{ste,soft}(T)$ is

$$\left(\frac{\mathrm{d}\mathcal{E}}{\mathrm{d}t}\right)_{ex}^{soft} = -n_H v \sigma_{ex}^{ste,soft} \equiv -\nu_{ex}^{ste,soft}. \tag{2.35}$$

Equating (2.34) and (2.35) yields

$$\ln \Lambda_{ex}^{soft} = \frac{4\pi\varepsilon_0^2 m v}{n_H e^4} \nu_{ex}^{ste,soft}. \tag{2.36}$$

2.2.4. Logarithmic factor

The logarithm factor due to soft inelastic collisions is

$$\ln \Lambda^{soft} = \frac{4\pi\varepsilon_0^2 m v}{n_H e^4} (\nu_{iz}^{sti,soft} + \nu_{ex}^{ste,soft}). \tag{2.37}$$

Remind that we deduce (2.37) by matching a function form of stopping power. That is to say, it does not originate from diverging nature of scattering cross-sections in small energy transfer limit like free–free Coulomb collisions (Rosenbluth *et al.* 1957).

In the $h \to 1$ limit, all collisions are soft. The logarithmic factor due to total inelastic collisions can be obtained by taking this limit, i.e. $\ln \Lambda^{tot} = \lim_{h\to 1} \ln \Lambda^{soft}$, since the test particle operator in the FPB is approximated to the FP. The hard collision part becomes $\ln \Lambda^{hard} = \ln \Lambda^{tot} - \ln \Lambda^{soft}$.

Figure 2 shows the smallness of the logarithmic factor for free-bound collisions. In fully ionised plasmas, the Coulomb logarithm measures the dominance of small angle scattering ($\ln \Lambda \gg 1$) and justifies neglect of higher order terms during derivation of the FP operator. In other words, such a system meets $(\partial f/\partial t)_c \approx -\nabla \cdot (f\langle \Delta \boldsymbol{v} \rangle) + 1/2 \nabla\nabla : (f\langle \Delta \boldsymbol{v} \Delta \boldsymbol{v} \rangle)$ since high-order terms like $\langle \Delta \boldsymbol{v} \Delta \boldsymbol{v} \Delta \boldsymbol{v} \rangle$ do not

https://doi.org/10.1017/S0022377826101329 Published online by Cambridge University Press

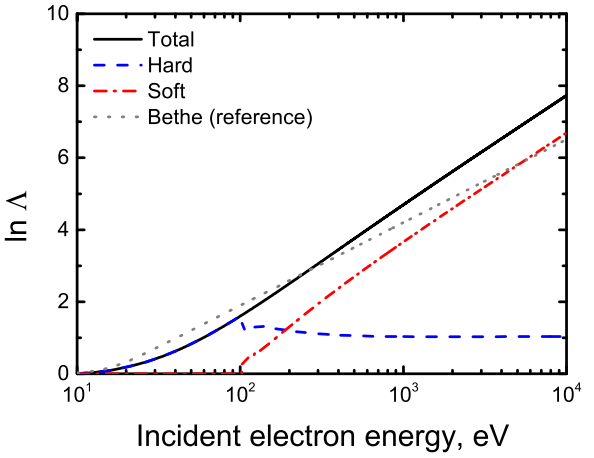


FIGURE 2. Logarithmic factor due to inelastic collisions, total (solid black), hard (blue dashed) and soft (red dash-dotted) with $h = 0.1$. Grey dotted line is the Bethe model extrapolated as a reference.

contain ln Λ. For inelastic collisions, however, the logarithmic factor is so small that the assumption required for the expansion is broken. In addition, the inelastic collisions are predominantly hard for low-energy particles. Such collisions need to be accounted for by (2.23).

2.2.5. Normalisation

Let $\tilde{\nu}_{iz}^{sti,soft} = \nu_{iz}^{sti,soft}\tau_c/mc^2$, $\tilde{\nu}_{ex}^{ste,soft} = \nu_{ex}^{ste,soft}\tau_c/mc^2$ and $\ln\tilde{\Lambda}^{soft} = n_H \ln\Lambda^{soft}/\, n_e \ln\Lambda$. Neglecting the tilde, the normalised logarithmic factor due to inelastic collisions $\ln\Lambda_{bound}$ is

$$\ln\Lambda^{soft} = \beta\left(\nu_{iz}^{sti,soft} + \nu_{ex}^{ste,soft}\right). \tag{2.38}$$

For $\mathcal{C}_{FP}^{soft}\{f_e\}$, we took a form given by Helander & Sigmar (2005). Using this form together with (2.25), (2.26) and (2.37), $2\pi p^2\mathcal{C}_{FP}^{soft}\{f_e\}$ becomes

$$2\pi p^2\mathcal{C}_{FP}^{soft}\{f_e\} = \frac{\partial}{\partial p} p\nu_S^{e,eb} F_e + \left(\nu_D^{e,eb} + \nu_D^{eH}\right)\mathcal{L}\{F_e\}, \tag{2.39}$$

where $\mathcal{L}$ is the Laplace operator (Helander & Sigmar 2005) and characteristic collisional frequencies are

$$\nu_S^{e,eb} = \frac{\gamma^2}{p^3}\ln\Lambda^{soft}, \tag{2.40}$$

$$\nu_D^{e,eb} = \frac{\gamma}{p^3}\ln\Lambda^{soft}, \tag{2.41}$$

$$\nu_D^{eH} = \frac{\gamma}{p^3}\chi\frac{n_H I_2^H(y)}{n_e\ln\Lambda}. \tag{2.42}$$

Here, ν_D^{eH} and $\nu_S^{e,eb}$ are shown in figures 3(*a*) and 3(*b*), respectively. All elastic collisions are accounted for by ν_D^{eH} in C_{FP}^{soft}. For inelastic collisions of low-energy

https://doi.org/10.1017/S0022377826101329 Published online by Cambridge University Press

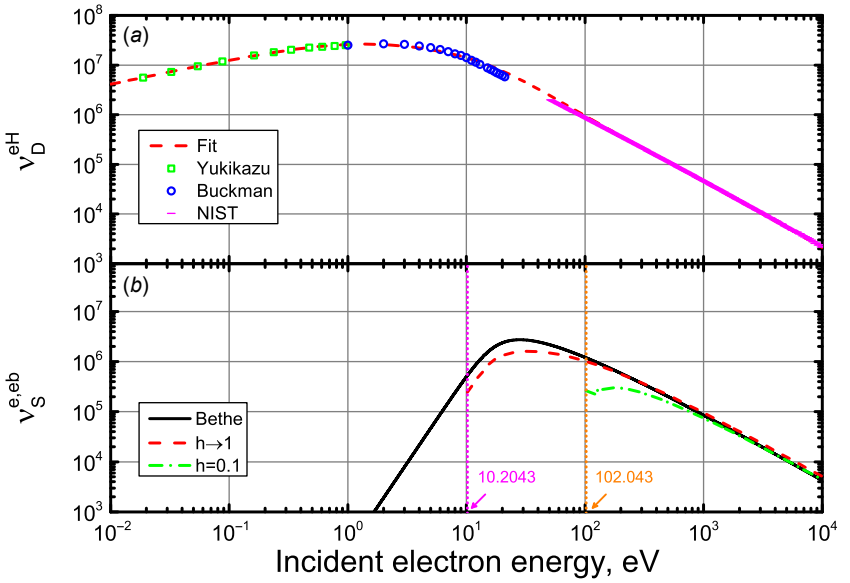


FIGURE 3. (*a*) Normalised deflection frequency and (*b*) slowing-down frequency as a function of incident electron energy. The legend of panel (*a*) is same as figure 1. Panel (*b*) is from the extrapolated Bethe model (Hesslow *et al.* 2017) (black solid), the FPB model in $h \to 1$ limit (red dashed) and with $h = 0.1$ (green dash-dotted). $n_e = 10^{16}$ m^{-3} and $n_H = 0.99 \cdot 10^{18}$ m^{-3}. Reprinted figure with permission from Lee *et al.* (2024), copyright 2025 by the American Physical Society.

electrons, the soft collisions represent only a fraction of all collisions and the associated frequency is therefore lower. In the $h = 0.1$ case, for instance, $\nu_S^{e,eb} = 0$ in $\mathcal{C}^{eH}$ and $\mathcal{B}^{eH}$ treats all inelastic collisions below 102.043 eV. This energy corresponds to $1/h$ of the minimal excitation energy for H. The 'continuous' soft collision energy loss is significantly reduced even above 102.043 eV. Nevertheless, the green curve goes to the red curve for high-energy electrons due to the dominating soft collisions over the hard collisions.

2.3. *Invariance in h*

The collision operator $\mathcal{C}^{eH}$ is invariant in the total particle source rate and total energy loss rate with respect to h, i.e. $\partial/\partial h[\int \mathrm{d}p\,\mathrm{d}\mu 2\pi p^2\ \mathcal{C}\{f_e\}] = \partial/\partial h[\int \mathrm{d}p\,\mathrm{d}\mu\ (\gamma - 1)2\pi p^2 \mathcal{C}\{f_e\}] = 0$. The invariance ensures the particle and energy conservation and, for a given distribution function, decouple an effect of energy loss allocation on electron acceleration from that of total energy loss.

2.3.1. Particle loss rate

Let us take an integral $\int \mathrm{d}p\,\mathrm{d}\mu$ on $2\pi p^2 \mathcal{C}^{eH}\{f_e\} = 2\pi p^2 \mathcal{C}_{FP}^{soft}\{f_e\} + 2\pi p^2 \mathcal{B}_{iz}^{hard}\{f_e\} + 2\pi p^2 \mathcal{B}_{ex}^{hard}\{f_e\}$. The term $\int \mathrm{d}p\,\mathrm{d}\mu 2\pi p^2 \mathcal{C}_{FP}^{soft}\{f_e\}$ automatically goes to 0 due to its convective–diffusive form. An integral $\int \mathrm{d}\mu$ on $2\pi p^2 \mathcal{B}_{iz}^{hard}\{f_e\}$ yields

$$\int \mathrm{d}\mu 2\pi p^2 \mathcal{B}_{iz}^{hard}\{f_e\} = n_H m c^3 \tau_c \frac{p}{\gamma}\left[\int_{p_{bnd}} \mathrm{d}p_1 \frac{\partial \sigma_{iz}}{\partial W}\frac{p_1}{\gamma_1} F_e^0(p_1)\right] - \nu_{iz}^{hard} F_e^0(p). \quad (2.43)$$

https://doi.org/10.1017/S0022377826101329 Published online by Cambridge University Press

For an integral $\int \mathrm{d}p$, change an integral variable from p to W and swap the order of integration, i.e. $\int \mathrm{d}p \int_{p_{bnd}} \mathrm{d}p_1 = 1/(mc^2) \int \mathrm{d}p_1 \int_0^{T-B-W_{bnd}} \mathrm{d}W$. Then, an integral part $\int_0^{T-B-W_{bnd}} \mathrm{d}W \partial \sigma_{iz}^{hard}/\partial W = \sigma_{iz} + \sigma_{iz}^{hard}$ is isolated. The result of taking an integral $\int \mathrm{d}p$ on (2.43) is independent of h, i.e.

$$\int \mathrm{d}p\, \mathrm{d}\mu 2\pi p^2 \mathcal{B}_{iz}^{hard}\{f_e\} = \int \mathrm{d}p_1\ (\nu_{iz} + \nu_{iz}^{hard}) F_e^0(p_1) - \int \mathrm{d}p\ \nu_{iz}^{hard} F_e^0(p)$$
$$= \int \mathrm{d}p\ \nu_{iz} F_e^0(p). \tag{2.44}$$

Using $\beta(p)\,\mathrm{d}p = \beta(p_{1n}^+)\,\mathrm{d}p_{1n}^+$, the excitation part is straightforward,

$$\int \mathrm{d}p\, \mathrm{d}\mu 2\pi p^2 \mathcal{B}_{ex,1s\to np}^{hard}\{f_e\} = \int \mathrm{d}p_{1n}^+ \left[\nu_{ex,1s\to np}^{hard}(p_{1n}^+) F_e^0(p_{1n}^+)\right]$$
$$- \int \mathrm{d}p \left[\nu_{ex,1s\to np}^{hard}(p) F_e^0(p)\right] = 0. \tag{2.45}$$

Finally, the outcome,

$$\int \mathrm{d}p\, \mathrm{d}\mu 2\pi p^2 \mathcal{C}^{eH}\{f_e\} = \int \mathrm{d}p\ \nu_{iz} F_e^0(p), \tag{2.46}$$

suggests the total particle loss is invariant in h.

2.3.2. Energy loss rate

Take an integral $\int \mathrm{d}p\, \mathrm{d}\mu \gamma$ on $2\pi p^2 \mathcal{C}_{FP}^{soft}$ and then the pitch angle scattering part automatically goes to 0. The remaining part is

$$\int \mathrm{d}p \gamma \partial_p (p \nu_S^{e,eb} F_e^0(p)) = \int \mathrm{d}p \left[-\nu_{iz}^{sti,soft}(T)\right] F_e^0(p) + \int \mathrm{d}p \left[-\nu_{ex}^{ste,soft}(T)\right] F_e^0(p). \tag{2.47}$$

Take an integral $\int \mathrm{d}\mu$ on the ionisation part in the Boltzmann operator to eliminate the scattering angle term,

$$\int \mathrm{d}\mu 2\pi p^2 \mathcal{B}_{iz}^{hard} = n_H m c^3 \tau_c \frac{p}{\gamma} \int_{p_{bnd}} \mathrm{d}p_1 \left[\frac{\partial \sigma_{iz}(W,T)}{\partial W} \frac{p_1}{\gamma_1} F_e^0(p_1)\right] - \nu_{iz}^{hard} F_e^0(p). \tag{2.48}$$

For an integral $\int \gamma\, \mathrm{d}p$, change an integral variable from p to W and swap the order of integration, i.e. $\int \mathrm{d}p \int_{p_{bnd}} \mathrm{d}p_1 = 1/(mc^2) \int \mathrm{d}p_1 \int_0^{T-B-W_{bnd}} \mathrm{d}W$. This isolates the integral of $\partial \sigma_{iz}(W,T)/\partial W$. From 0 to $(T-B)/2$, the result of the integral is $\int_0^{(T-B)/2} \mathrm{d}W \gamma \partial \sigma_{iz}(W,T)/\partial W = 1/(mc^2)\sigma_{iz}^{sti} + (1-b')\sigma_{iz}$. Then, take a variable transformation from W to $T-B-\tilde{W}$ on the remaining part,

$$\int_0^{T-B-W_{bnd}} \mathrm{d}W \gamma \frac{\partial \sigma_{iz}(W,T)}{\partial W} = \frac{1}{mc^2}\sigma_{iz}^{sti} + (1-b')\sigma_{iz}$$
$$+ \int_{W_{bnd}}^{(T-B)/2} \mathrm{d}\tilde{W} \gamma (T-B-\tilde{W}) \frac{\partial \sigma_{iz}(\tilde{W},T)}{\partial \tilde{W}}. \tag{2.49}$$

https://doi.org/10.1017/S0022377826101329 Published online by Cambridge University Press

The outcome of $\int \mathrm{d}p\gamma$ on (2.48), resolving $\nu_{iz}^{hard} = n_H c\tau_c p/\gamma \int_{W_{bnd}}^{(T-B)/2} \mathrm{d}\tilde{W}\partial\sigma_{iz}(\tilde{W}, T)/\partial\tilde{W}$, becomes

$$\begin{aligned}\int \mathrm{d}\mu\, \mathrm{d}p\gamma 2\pi p^2 \mathcal{B}_{iz}^{hard} &= \int \mathrm{d}p_1 \left[\nu_{iz}^{sti} + (1-b')\nu_{iz}\right] F_e^0(p_1) + n_H c\tau_c \int \mathrm{d}p \frac{p}{\gamma} F_e^0(p) \\ &\quad \times \left[\int_{W_{bnd}}^{(T-B)/2} d\tilde{W}(\gamma(T-B-\tilde{W}) - \gamma(T)) \frac{\partial\sigma_{iz}(\tilde{W}, T)}{\partial\tilde{W}}\right] \\ &= \int \mathrm{d}p \left[\nu_{iz}^{sti,soft} + (1-b')\nu_{iz}\right] F_e^0(p).\end{aligned} \tag{2.50}$$

Take a $\int \mathrm{d}\mu$ on the excitation part ($1s \to np$ transition) in the Boltzmann operator,

$$\int \mathrm{d}\mu 2\pi p^2 \mathcal{B}_{ex,1s\to np}^{hard} = \nu_{ex,1s\to np}^{hard}(p_{1n}^+) \frac{\beta(p)}{\beta(p_{1n}^+)} F_e^0(p_{1n}^+) - \nu_{ex,1s\to np}^{hard}(p) F_e^0(p). \tag{2.51}$$

For $\int \mathrm{d}p\gamma$, use $\beta(p_{1n}^+)\,\mathrm{d}p_{1n}^+ = \beta(p)\,\mathrm{d}p$,

$$\begin{aligned}\int \mathrm{d}\mu\, \mathrm{d}p\gamma 2\pi p^2 \mathcal{B}_{ex,1s\to np}^{hard} &= \int \mathrm{d}p_{1n}^+ \gamma \left[\nu_{ex,1s\to np}^{hard}(p_{1n}^+) F_e^0(p_{1n}^+)\right] \\ &\quad - \int \mathrm{d}p\gamma \left[\nu_{ex,1s\to np}^{hard}(p) F_e^0(p)\right] \\ &= \int \mathrm{d}p[(\gamma(T-E_{1n}) - \gamma(T))]\nu_{ex,1s\to np}^{hard} F_e^0(p) \\ &= \int \mathrm{d}p \left[-\nu_{ex,1s\to np}^{ste,hard}\right] F_e^0(p).\end{aligned} \tag{2.52}$$

Finally, (2.46), (2.47), (2.50) and (2.52) yield the outcome,

$$\int \mathrm{d}p\, \mathrm{d}\mu(\gamma - 1)2\pi p^2 \mathcal{C}^{eH}\{f_e\} = \int \mathrm{d}p \left[-b'\nu_{iz} - \nu_{ex}^{ste}\right] F_e^0(p), \tag{2.53}$$

which suggests the total energy loss is invariant in h.

2.4. *Collisions with free electrons and ions*

We describe the kinetic model for collisions with free electrons and ions for completeness of this paper. The majority of free electrons are assumed *a posteriori* to be Maxwellian. The justification is essential for applying it to weakly ionised plasmas and will therefore be verified through numerical simulation in § 2.4.4.

The FP operator is used to account for the Coulomb collisions with free electrons and ions:

$$2\pi p^2 \mathcal{C}_{FP}\{f_e\} = 2\pi p^2 \mathcal{C}_{FP}^{e,i}\{f_e\} + 2\pi p^2 \mathcal{C}_{FP}^{e,ef}\{f_e\}. \tag{2.54}$$

The collisions with ions are described by the Lorentz operator (Helander & Sigmar 2005):

$$2\pi p^2 \mathcal{C}_{FP}^{e,i}\{f_e\} = \nu_D^{ei} \mathcal{L}\{F_e\}. \tag{2.55}$$

The deflection frequency is

$$\nu_D^{ei} = \frac{\gamma}{p^3} \frac{\ln \Lambda_{free}}{\ln \Lambda}. \tag{2.56}$$

https://doi.org/10.1017/S0022377826101329 Published online by Cambridge University Press

We take $\ln \Lambda_{free}$ from (29) of Breizman *et al.* (2019),

$$\ln \Lambda_{free} = \frac{1}{2} \ln \frac{m^2 c^2 (\gamma^2 - 1)(\gamma - 1)}{2\hbar^2 \omega_p^2 \gamma^2}, \tag{2.57}$$

where $\omega_p \equiv \sqrt{n_e e^2/(m\varepsilon_0)}$ is the plasma frequency and $\hbar$ is the Planck constant. While this form adequately describes a stopping power felt by energetic electrons from Coulomb collisions, it is unsuitable for cold electrons moving at speeds below the thermal velocity; it exhibits correct independence from electron temperature in the high-energy regime due to plasma wave excitation (Bohm & Gross 1949; Solodov & Betti 2008). Accordingly, an interpolation towards the Coulomb logarithm for thermal electrons, based on Richardson (2019), was applied.

For collisions with free electrons, we linearise $\mathcal{C}_{FP}^{e,ef}$ because nonlinear terms are negligible:

$$2\pi p^2 \mathcal{C}_{FP}^{e,ef}\{f_e\} \approx 2\pi p^2 \mathcal{C}_{FP}^{e,ef}\{f_e,\, f_M\} + 2\pi p^2 \mathcal{C}_{FP}^{e,ef}\{f_M,\, f_e\}, \tag{2.58}$$

where f_M is the Maxwell distribution.

2.4.1. Test particle part

The test particle operator has a form given by Papp *et al.* (2011):

$$2\pi p^2 \mathcal{C}_{FP}\{f_e,\, f_M\} = \frac{\partial}{\partial p}\left[p\left(\nu_S^{e,ef} - \nu_\parallel^{e,ef}\right) + \frac{1}{2} p^2 \nu_\parallel^{e,ef} \frac{\partial}{\partial p} \right] F_e + \left(\nu_D^{e,ef} + \nu_D^{ei}\right) \mathcal{L}\{F_e\}. \tag{2.59}$$

This operator is suitable for arbitrary electron energies. The collision frequencies are

$$\nu_S^{e,ef} = \frac{G(X_G)}{\bar{T}_e p} \frac{\ln \Lambda_{free}}{\ln \Lambda}, \tag{2.60}$$

$$\nu_\parallel^{e,ef} = 2\frac{\gamma}{p^3} G(X_G) \frac{\ln \Lambda_{free}}{\ln \Lambda}, \tag{2.61}$$

$$\nu_D^{e,ef} = \frac{\gamma}{p^3} (\Phi(X_G) - G(X_G) + \bar{T}_e \beta^2) \frac{\ln \Lambda_{free}}{\ln \Lambda}, \tag{2.62}$$

$$\nu_D^{ei} = \frac{\gamma}{p^3} \frac{\ln \Lambda_{free}}{\ln \Lambda}, \tag{2.63}$$

where $\bar{T}_e = T_e/mc^2$, $X_G = v/v_{th}$ is the velocity normalised by the thermal velocity $v_{th} = \sqrt{2T_e/m}$, $G(X_G)$ is the Chandraseckhar function and $\Phi(X_G)$ is the error function.

2.4.2. Field particle part

The field particle operator is necessary to explicitly justify the background Maxwell assumption because the exponential factor is not negligible at the core.

The field particle operator has a form given by Li & Ernst (2011):

$$\begin{aligned} 2\pi p^2 \mathcal{C}\{f_M,\, f_e\} = \frac{1}{2\pi} \int \mathrm{d}p' \, \mathrm{d}\mu' \Bigg[\frac{1}{\beta_T^4} \Bigg(\left(\beta^2 + \beta'^2\right) \frac{4K(\kappa)}{\lambda} - 2\lambda E(\kappa) \\ - \left(\beta^2 - \beta'^2\right)^2 \frac{2E(\kappa)}{\lambda^3(1-\kappa^2)} \Bigg) - \frac{2}{\beta_T^2} \frac{4K(\kappa)}{\lambda} \Bigg] \bar{F}_M(\boldsymbol{p}) F_e(\boldsymbol{p}') + \frac{2}{p^2} \bar{F}_M(\boldsymbol{p}) F_e(\boldsymbol{p}), \end{aligned} \tag{2.64}$$

https://doi.org/10.1017/S0022377826101329 Published online by Cambridge University Press

where $\bar{F}_M = 2\pi p^2 f_M / n_e$, $\beta_T = v_T/c$, $\lambda^2 = (\beta_\perp + \beta'_\perp)^2 + (\beta_\parallel - \beta'_\parallel)^2$ with $\beta_\perp = \beta\sqrt{1-\mu^2}$ and $\beta_\parallel = \beta\mu$, and $\kappa^2 = 4\beta_\perp\beta'_\perp/\lambda^2$. Here, K and E are the complete elliptic integral of the first and second kinds, respectively.

2.4.3. Conservation laws

The conservation laws are approximately satisfied with the free–free collision operator (2.58). The relativistic operator that was matched to obtain (2.59) (Papp *et al.* 2011) originates from the Beliaev–Budker kernel (Beliaev & Budker 1956; Landau *et al.* 1981) by taking the Taylor expansion up to the second order (Sandquist *et al.* 2006). However, the only correction given by this matching from the semi-relativistic operator (Helander & Sigmar 2005) is the $\bar{T}_e\beta^2$ term in (2.62) that is much smaller than $\Phi(X_G) \to 1$ for energetic electrons due to $\bar{T}_e \ll 1$. Therefore, both operators can be represented by the Landau kernel (Landau *et al.* 1981) and conservation laws are approximately satisfied (Landau *et al.* 1981) in cold weakly ionised plasmas. Note that the Landau kernel is indeed semi-relativistic and appropriate if one of the colliding particles is non-relativistic (Braams & Karney 1987).

2.4.4. Verification of the Maxwellian assumption

The 'core' Maxwell assumption can be guaranteed if $n_e \ln \Lambda_{free} \gg n_H \ln \Lambda_{bound}$, where $\ln \Lambda_{free}$ is the Coulomb logarithm for free–free collisions and $\ln \Lambda_{bound}$ is the logarithmic factor for free–bound collisions. This condition is evidently satisfied below 100 eV because $\ln \Lambda_{bound}$ felt by a majority of electrons is $\ln \Lambda^{soft}$ and thus is vanishingly small (see red curve in figure 2). Therefore, the lower energy part of the population is predominantly Maxwellian. The argument is only true for the background electron distribution, not for the entire electron distribution.

The adequacy of the background Maxwellian assumption is numerically verified by confirming whether the Maxwell distribution function is sustained or not under the effect of free-bound collisions accounted by $\mathcal{C}$. The numerical simulation is carried out by initiating F_M and then evolving it for 20 μs under the weakly ionised condition where the ionisation fraction $\alpha \equiv n_e/(n_H + n_e) = 1\,\%$. Figure 4 shows resulting F_e^0. The black curve aligns well with the red curve. This good agreement indicates inelastic collisions do not distort F_e^0 as severely as violate the Maxwell assumption. In this specific example, a total friction of free–bound collision dominates free–free collision due to $n_e \ln \Lambda_{free} \ll n_H \ln \Lambda^{tot}$. Nonetheless, the Maxwell assumption is valid because the majority of electrons do not experience inelastic collisions at all, i.e. $n_e \ln \Lambda_{free} \gg n_H \ln \Lambda^{soft}$. Indeed, free–bound collisions are strong, as seen by the blue curve, which clearly deviates from Maxwellian due to the misuse of the FP operator. For the verification, the ionising avalanche is regulated by adopting the test particle part in $\mathcal{C}^{eH}$, while the field particle part is included in $\mathcal{C}_{FP}$ for the low energy population. The detailed description for the implementation is in § 3.

2.5. *Non-diffusive electron acceleration mechanism*

The free–free and free–bound interactions exhibit significantly different interaction distances. This difference distinguishes the electron acceleration mechanisms. For free–free collisions, all electrons feel the interactions due to the long-range nature in the single particle description. In the kinetic description, electrons with the same energy have the same slowing down frequency. The FP operator takes into account disparities in the momentum exchanges using the velocity space diffusion frequency. Through the diffusion mechanism within the narrow singular layer across

https://doi.org/10.1017/S0022377826101329 Published online by Cambridge University Press

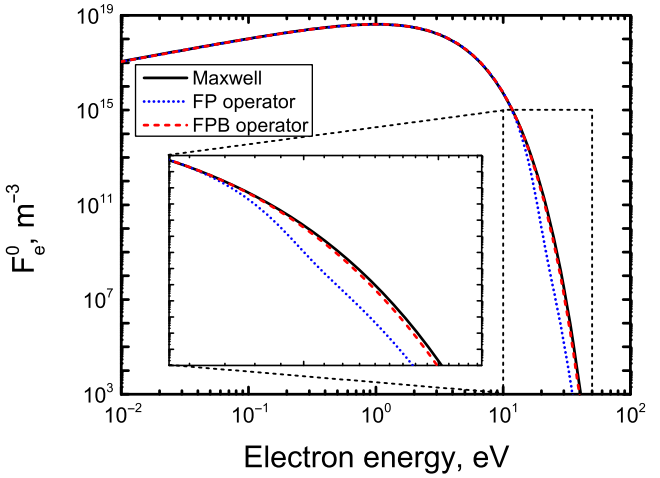


FIGURE 4. Maxwell distribution function (black solid curve) and F_e^0 that evolves for 20 μs from the black curve with the FPB (red dashed curve, $h = 0.1$) and FP (blue dotted curve, $h = 0.99$) operators. $(n_H + n_e) = 10^{18}$ m^{-3}, $T_e = 1$ eV and $\alpha = 1$ %.

the critical momentum in phase space, the upward Dreicer flow can form under the effect of electric field, below which the mean frictional force exceeds the electric force. In contrast, the range of interaction is short for free–bound inelastic collisions due to a screened charge of neutrals in the single particle description. Therefore, some electrons can accelerate freely without undergoing inelastic collisions whenever they encounter a neutral particle. In the kinetic description, this mechanism is evidently distinct from the diffusive process and occurs over the electrons' acceleration trajectories in the low-energy region of phase space, where most inelastic collisions are hard so should be described by the Boltzmann operator; electrons can share the slowing down frequency only if the associated energy transfer is very small compared with their energy, i.e. for soft collisions.

Such accounting of binary nature of inelastic collisions dramatically changes the critical energy crossing for free acceleration. This is clarified in figure 5 that shows mean frictional forces considered by the FP operator for the ionisation fractions $\alpha =$ 1 %, 2 %, 5 % and 11 %. The corresponding parameters are close to that of standard Ohmic discharge in KSTAR tokamak (Yoo *et al.* 2018; Lee *et al.* 2023*a*) and ITER plasma initiation (de Vries & Gribov 2019). Note that the mean frictional force is shared by electrons with the same energy through the slowing down frequency in each model. Other collisions considered by the binary Boltzmann operator are excluded in this computation. If the FP operator describes all collisions (blue or black curve), electron runaway begins at the critical energy crossing (e.g. see blue circle in figure 5*a*). However, the FPB treatment can eliminate the crossing as shown in figure 5(*a*) if the ionisation fraction is sufficiently low. In this case, the Dreicer condition (Dreicer 1959) is completely satisfied for some electrons: all electrons that do not experience hard inelastic collisions are runaway. Even in less extreme cases, the proposed model significantly modifies the critical energy by an order of magnitude (figure 5*b*) or allows the virtual free acceleration (figure 5*c*). The increased ionisation fraction makes the change in the critical energy less significant. Yet, the frictional force can be notably reduced even in this case (figure 5*d*). In

https://doi.org/10.1017/S0022377826101329 Published online by Cambridge University Press

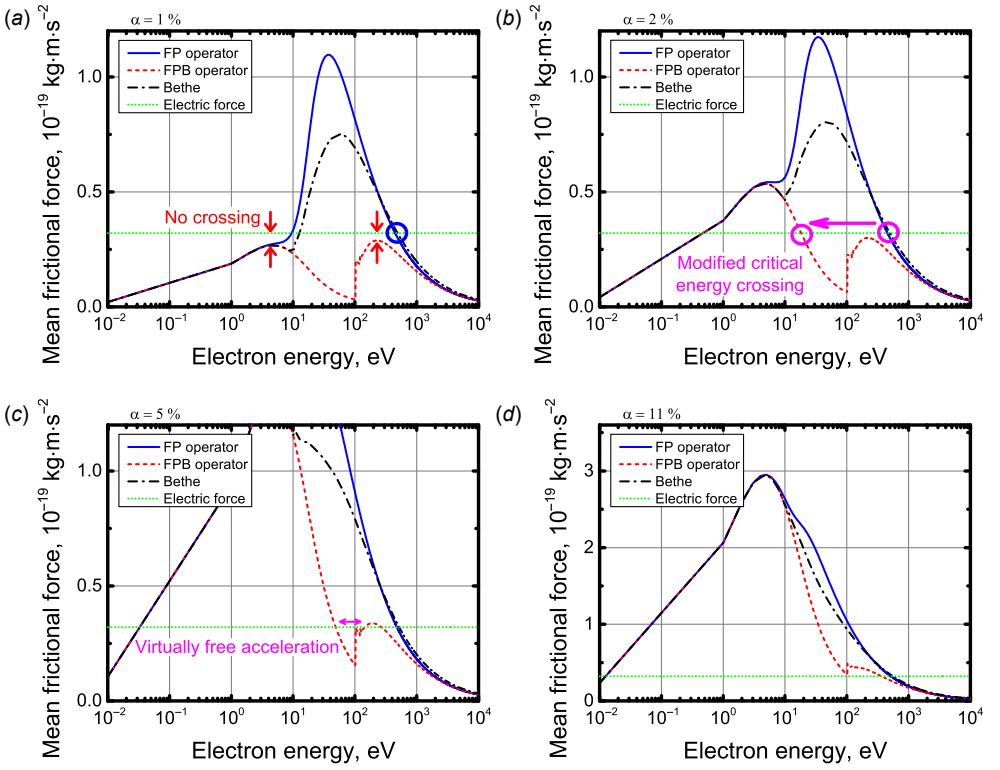


FIGURE 5. Mean frictional force considered by the FP operator as a function of incident electron energy. Free–bound collisions are from the extrapolated Bethe model (Hesslow *et al.* 2017) (black dashed dotted curve), the FPB model in $h \to 1$ limit, same to the FP model (blue solid curve), and with $h = 0.1$ (red dashed curve). Green dotted curve is the electric force. $n_e + n_H = 10^{18}$ m^{-3}, $E = 0.2$ Vm^{-1}, $T_e = 5$ eV and $\ln \Lambda_{free} = 15$. $\alpha = 1\,\%,\ 2\,\%,\ 5\,\%$ and $11\,\%$ for panels (*a*), (*b*), (*c*) and (*d*), respectively.

summary, the proposed model captures the non-diffusive Dreicer mechanism and allows for variations in the critical energy beyond the mean-friction approximation. Another noteworthy aspect is the associated diffusion with soft inelastic collisions, which will be addressed in a future study.

3. Numerical implementation

We implement the FPB operator in the self-consistent kinetic simulation (Aleynikov & Breizman 2017) using FiPy, a finite volume partial differential equation (PDE) solver (Guyer, Wheeler & Warren 2009). In FiPy, the discretisation of $\mathcal{B}^{hard}\{F_e\}$ should be given in a volume-averaged form to ensure the particle conservation by

$$\int_{p_{l,i}}^{p_{r,i}} \mathrm{d}p \int_{\mu_{l,j}}^{\mu_{r,j}} \mathrm{d}\mu \mathcal{B}^{hard}\{F_e\} \approx \mathcal{B}^{hard}\{F_e\}(p_i, \mu_j)\Delta p_i \Delta \mu_j, \tag{3.1}$$

where (p_i, μ_j) is the (i, j)th cell centred coordinate, l and r denote the left and right side cell face, respectively, $\Delta p_i = p_{r,i} - p_{l,i}$, and $\Delta \mu_j = \mu_{r,j} - \mu_{l,j}$.

https://doi.org/10.1017/S0022377826101329 Published online by Cambridge University Press

3.1. *Discretisation of* $\mathcal{B}_{iz}^{hard}\{F_e\}$

In the integral term in (2.23), (p_1, μ_1) and (p, μ) denote the continuous phase-space coordinates of electrons before and after collisions, respectively. During the numerical discretisation, these coordinates are replaced with $(p_k, \mu_{l'})$ for incident electrons, and (p_i, μ_j) for scattered and ejected electrons. A complete analytic integration is only possible in the (p_i, μ_j)-coordinate because $F_e(p_k, \mu_{l'})$ is discretised. Hence, after discretising $\mathcal{B}_{iz}^{hard}\{F_e\}$ in the (p_i, μ_j)-coordinate and erasing the dependence on p_i and μ_j through summation, we will find a proper discretisation of the $(p_k, \mu_{l'})$-coordinate required for the particle conservation.

Consider taking an integral $\int_{\mu_{l,j}}^{\mu_{r,j}} \mathrm{d}\mu$ on $\mathcal{B}_{iz}^{hard}\{F_e\}$ and discretise the μ-integral using the relation,

$$\begin{aligned}\int_{\mu_{l,j}}^{\mu_{r,j}} \mathrm{d}\mu \frac{\mathcal{H}((1-\mu^2)(1-\mu_1^2)-(\mu^*-\mu\mu_1)^2)}{\sqrt{(1-\mu^2)(1-\mu_1^2)-(\mu^*-\mu\mu_1)^2}} \\ = \sin^{-1}\left[\min_2\left(-1, \frac{\mu_{r,j}-\mu_1\mu^*}{\sqrt{(1-\mu_1^2)(1-\mu^{*2})}}, 1\right)\right] \\ - \sin^{-1}\left[\min_2\left(-1, \frac{\mu_{l,j}-\mu_1\mu^*}{\sqrt{(1-\mu_1^2)(1-\mu^{*2})}}, 1\right)\right].\end{aligned} \tag{3.2}$$

Here, $\sum_j$ erases the μ_j-dependence owing to $\mu_{l,0} = -1$ and $\mu_{r,-1} = 1$ with the particle conservation, where the index -1 indicates the last one. Subsequently, discretise the p-integral by taking $\int_{p_{l,i}}^{p_{r,i}} \mathrm{d}p$ on $\sum_j \int_{\mu_{l,j}}^{\mu_{r,j}} \mathrm{d}\mu \mathcal{B}_{iz}^{hard}\{F_e\}$ and using the relation,

$$\int_{p_{l,i}}^{p_{r,i}} \mathrm{d}p\left[mc^2\frac{p}{\gamma}\frac{\partial\sigma_{iz}(W,T)}{\partial W}\right] = \Delta\sigma_{iz}(w_{r,i}, T) - \Delta\sigma_{iz}(w_{l,i}, T), \tag{3.3}$$

where $w_{r,i} = (\sqrt{p_{r,i}^2+1}-1)/b'$, $w_{l,i} = (\sqrt{p_{l,i}^2+1}-1)/b'$ and $\Delta\sigma_{iz}(w, T)$ is

$$\begin{aligned}\Delta\sigma_{iz}(w,T) &\equiv \int_0^w \mathrm{d}w \frac{\partial\sigma_{iz}(W,T)}{\partial W} \\ &= \frac{4\pi a_0^2\alpha_{fs}^4 N}{(\beta_t^2+\beta_u^2+\beta_b^2)2b'}\left\{\bar{D}(0,w)\left[\ln\left(\frac{\beta_t^2}{1-\beta_t^2}\right)-\beta_t^2-\ln(2b')\right]\right. \\ &\quad + \left(2-\frac{N_i}{N}\right)\left[1-\frac{1}{t}+\frac{1}{t-w}-\frac{1}{w+1}\right. \\ &\quad \left.\left.-\ln\left((w+1)\frac{t}{t-w}\right)\frac{1}{t+1}\frac{1+2t'}{(1+t'/2)^2}+\frac{bt'^2}{(1+t'/2)^2}w\right]\right\}.\end{aligned} \tag{3.4}$$

Here,

$$\begin{aligned}\bar{D}(0,w) = \frac{1}{N}\int_0^w \frac{1}{1+w}\frac{\mathrm{d}f}{\mathrm{d}w}\mathrm{d}w = \frac{b}{2}\left[1-\frac{1}{(1+w)^2}\right]+\frac{c}{3}\left[1-\frac{1}{(1+w)^3}\right] \\ + \frac{d}{4}\left[1-\frac{1}{(1+w)^4}\right]+\frac{e}{5}\left[1-\frac{1}{(1+w)^5}\right].\end{aligned}$$

https://doi.org/10.1017/S0022377826101329 Published online by Cambridge University Press

Swapping the order of integration with p_1, $\sum_i$ erases the p_i-dependence:

$$\begin{aligned}
&\sum_i \int_{p_{pnd}} \mathrm{d}p_1\, \mathrm{d}\mu_1 \Big[\Delta\sigma_{iz}(w_{r,i}, T) - \Delta\sigma_{iz}(w_{l,i}, T)\Big] \\
&\quad = \int \mathrm{d}p_1\, \mathrm{d}\mu_1 \sum_{i<i^*} \Big[\Delta\sigma_{iz}(w_{r,i}, T) - \Delta\sigma_{iz}(w_{l,i}, T)\Big] \\
&\quad = \int \mathrm{d}p_1 \mathrm{d}\mu_1 \Big[\sigma_{iz}(T) + \sigma_{iz}^{hard}(T)\Big], \qquad (3.5)
\end{aligned}$$

where we replace $\Delta\sigma_{iz}(w_{l,0}, T)$ with $\Delta\sigma_{iz}(0, T)$, $\Delta\sigma_{iz}(w_{r,i^*}, T)$ with $\Delta\sigma_{iz}(t - w_{bnd} - 1, T)$, and i^* satisfies $w_{l,i^*} < t - w_{bnd} - 1$ and $w_{l,i^*+1} \geqslant t - w_{bnd} - 1$. Then, the ionisation part reduces to

$$\begin{aligned}
&\sum_{i,j} \int_{p_{l,i}}^{p_{r,i}} \mathrm{d}p \int_{\mu_{l,j}}^{\mu_{r,j}} \mathrm{d}\mu \mathcal{B}_{iz}^{hard}\{F_e\} \\
&\quad = \sum_{k,l'} \int_{p_{l,k}}^{p_{r,k}} \int_{\mu_{l,l'}}^{\mu_{r,l'}} \Big[(\nu_{iz}(T_k) + \nu_{iz}^{hard}(T_k)) F_e(p_k, \mu_{l'})\Big] \mathrm{d}p_k\, \mathrm{d}\mu_{l'} \\
&\qquad - \sum_{i,j} \int_{p_{l,i}}^{p_{r,i}} \int_{\mu_{l,j}}^{\mu_{r,j}} \Big[\nu_{iz}^{hard}(T_i)) F_e(p_i, \mu_j)\Big] \mathrm{d}p_i\, \mathrm{d}\mu_j. \qquad (3.6)
\end{aligned}$$

We discretise $\int_{p_{l,k}}^{p_{r,k}} \mathrm{d}p_k [\nu_{iz}(T_k) + \nu_{iz}^{hard}(T_k)) F_e(p_k, \mu_{l'})]$ grounded in the fact that $F_e(p_k, \mu_{l'})$ shows the exponential dependence on p_k, and both of $\nu_{iz}(T_k)$ and $\nu_{iz}^{hard}(T_k)$ have the algebraic dependence on p_k, i.e. $|\partial_p \ln(F_e)| \gg |\partial_p \ln(\nu_{iz})|$ and $|\partial_p \ln(F_e)| \gg |\partial_p \ln(\nu_{iz}^{hard})|$:

$$\int_{p_{l,k}}^{p_{r,k}} \mathrm{d}p_k \nu_{iz}(T_k) F_e(p_k, \mu_{l'}) \approx \nu_{iz}(T_k) F_e(p_k, \mu_{l'}) \Delta p_k, \qquad (3.7)$$

$$\int_{p_{l,k}}^{p_{r,k}} \mathrm{d}p_k \nu_{iz}^{hard}(T_k) F_e(p_k, \mu_{l'}) \approx \nu_{iz}^{hard}(T_k) F_e(p_k, \mu_{l'}) \Delta p_k. \qquad (3.8)$$

An exception where the condition $|\partial_p \ln(F_e)| \gg |\partial_p \ln(\nu_{iz})|$ can be severely broken and influence the discretisation is nearby $T \approx B$ due to onset of ionising collisions. We replace $\Delta p_{k^*} = p_{r,k^*} - p_{l,k^*}$ in (3.7) and (3.8) with $\Delta p_{k^*} = p_{r,k^*} - \sqrt{(b'+1)^2 - 1}$, where k^* satisfies $T_{r,k^*} > B$ and $T_{l,k^*} < B$. The remaining $\mu_{l'}$ part is straightforward: $\int_{\mu_{l,l'}}^{\mu_{r,l'}} \mathrm{d}\mu_{l'} F_e(p_k, \mu_{l'}) = F_e(p, \mu_{l'}) \Delta\mu_{l'}$. Finally, the fully discretised form of $\mathcal{B}_{iz}^{hard}\{F_e\}$ is

$$\mathcal{B}_{iz}^{hard}\{F_e\}(p_i, \mu_j) = \sum_{k,l'} \Big[\mathcal{B}_{iz}^{hard}\{F_e\}(p_i, \mu_j)\Big]_{k,l'} \Delta p_k \Delta\mu_{l'} - \nu_{iz}^{hard}(p_i) F_e(p_i, \mu_j), \qquad (3.9)$$

where

$$\begin{aligned}
[\mathcal{B}_{iz}^{hard}\{F_e\}(p_i, \mu_j)]_{k,l'} = \frac{1}{\Delta p_i \Delta\mu_j} \Bigg[&\Bigg\{ \frac{1}{\pi} \Bigg(\sin^{-1} \Bigg[\min_2 \Bigg(-1, \frac{\mu_{r,j} - \mu_1 \mu^*}{\sqrt{(1-\mu_1^2)(1-\mu^{*2})}}, 1 \Bigg) \Bigg] \\
&- \sin^{-1} \Bigg[\min_2 \Bigg(-1, \frac{\mu_{l,j} - \mu_1 \mu^*}{\sqrt{(1-\mu_1^2)(1-\mu^{*2})}}, 1 \Bigg) \Bigg] \Bigg) - \frac{\Delta\mu_j}{2} \Bigg\} \frac{1}{1 + \frac{0.1}{p_i}} + \frac{\Delta\mu_j}{2} \Bigg] \\
&\times \Big(\Delta\nu_{iz}(w_{r,i}, T_k) - \Delta\nu_{iz}(w_{l,i}, T_k)\Big) F_e(p_k, \mu_{l'}) \qquad (3.10)
\end{aligned}$$

https://doi.org/10.1017/S0022377826101329 Published online by Cambridge University Press

and $\Delta\nu_{iz} = n_H c\tau_c \Delta\sigma_{iz}(w_i, T_k)\beta_k$.

3.2. *Discretisation of* $\mathcal{B}^{hard}_{ex}\{F_e\}$

Consider $\int_{p_{l,i}}^{p_{r,i}} \mathrm{d}p$ on the source term of $\mathcal{B}^{hard}_{ex,1s\to np}\{F_e\}$ and discretise the p-integral,

$$\begin{aligned}
&\int_{p_{l,i}}^{p_{r,i}} \mathrm{d}p_i \frac{\nu^{hard}_{ex,1s\to np}(p^+_{1n})}{2} \frac{\beta(p_i)}{\beta(p^+_{1n})} F^0_e(p^+_{1n}) \\
&\quad = \sum_k \int_{p_{l,i}}^{p_{r,i}} \mathrm{d}p_i \int_{p_{l,k}}^{p_{r,k}} \mathrm{d}p_k \left[\frac{\nu^{hard}_{ex,1s\to np}(p_k)}{2} \frac{\beta(p_i)}{\beta(p_k)} F^0_e(p_k) \frac{\mathrm{d}T_k}{\mathrm{d}p_k} \delta(T_k - W_i - E_{1n}) \right] \\
&\quad = \sum_k \int_{p_{l,k}}^{p_{r,k}} \mathrm{d}p_k \left[\frac{\nu^{hard}_{ex,1s\to np}(p_k)}{2} F^0_e(p_k) \right] \left[\int_{W_{l,i}}^{W_{r,i}} \mathrm{d}W_i \delta(T_k - W_i - E_{1n}) \right] \qquad (3.11)
\end{aligned}$$

Here, we use the integral representation as the first step and interchange the order of integration as the second step. Suppose we just take $\int_{W_{l,i}}^{W_{r,i}} \mathrm{d}W_i \delta(T_k - W_i - E_{1n}) = 1$. In that case, the particle conservation is adequate but the ith cell-centred energy W_i is not equal to $T_k - E_{1n}$. To overcome this drawback, $\delta(T_k - W_i - E_{1n})$ is smoothed as meeting

$$\Delta\hat{W}^{1n}_{i-1,k} + \Delta\hat{W}^{1n}_{i,k} + \Delta\hat{W}^{1n}_{i+1,k} = 1, \qquad (3.12)$$

$$\Delta\hat{W}^{1n}_{i-1,k} W_{i-1} + \Delta\hat{W}^{1n}_{i,k} W_i + \Delta\hat{W}^{1n}_{i+1,k} W_{i+1} = T_k + E_{1n}, \qquad (3.13)$$

where $\Delta\hat{W}^{1n}_{i,k} \equiv \int_{W_{l,i}}^{W_{r,i}} \mathrm{d}W_i \hat{\delta}(T_k - W_i - E_{1n})$ and $\hat{\delta}$ is the smoothed Dirac-delta function. If $W_{l,i} < T_k - E_{1n} < W_i$, set $\Delta\hat{W}^{1n}_{i+1,k} = 0$ and then,

$$\Delta\hat{W}^{1n}_{i-1,k} = \frac{W_i - T_k + E_{1n}}{W_i - W_{i-1}}, \; \Delta\hat{W}^{1n}_{i,k} = \frac{T_k - E_{1n} - W_{i-1}}{W_i - W_{i-1}}. \qquad (3.14)$$

If $W_i < T_k - E_{1n} < W_{r,i}$, set $\Delta\hat{W}^{1n}_{i-1,k} = 0$ and then,

$$\Delta\hat{W}^{1n}_{i,k} = \frac{W_{i+1} - T_k + E_{1n}}{W_{i+1} - W_i}, \; \Delta\hat{W}^{1n}_{i+1,k} = \frac{T_k - E_{1n} - W_i}{W_{i+1} - W_i}. \qquad (3.15)$$

If $0 < T_k - E_{1n} < W_{l,0}$, just set $\Delta\hat{W}^{1n}_{0,k} = 1$, assuming the energy loss due to this approximation is negligible. After skipping the trivial μ-discretisation, we take $\sum_i$ to erase the i-dependence. Then,

$$\begin{aligned}
\sum_{i,j} \int_{p_{l,i}}^{p_{r,i}} \mathrm{d}p_i \int_{\mu_{l,j}}^{\mu_{r,j}} \mathrm{d}\mu_j \mathcal{B}^{hard}_{ex,1s\to np}\{F_e\} &= \sum_k \int_{p_{l,k}}^{p_{r,k}} \mathrm{d}p_k \left[\nu^{hard}_{ex,1s\to np}(p_k) F^0_e(p_k) \right] \\
&\quad - \sum_i \int_{p_{l,i}}^{p_{r,i}} \mathrm{d}p_i \left[\nu^{hard}_{ex,1s\to np}(p_i) F^0_e(p_i) \right]. \qquad (3.16)
\end{aligned}$$

We discretise $\int_{p_{l,k}}^{p_{r,k}} \mathrm{d}p_k [\nu^{hard}_{ex,1n\to np}(p_k) F^0_e(p_k)]$ similarly to (3.8),

$$\int_{p_{l,k}}^{p_{r,k}} \mathrm{d}p_k \nu^{hard}_{ex,1s\to np}(p_k) F^0_e(p_k) \approx \nu^{hard}_{ex,1s\to np}(p_k) F^0_e(p_k) \Delta p_k. \qquad (3.17)$$

https://doi.org/10.1017/S0022377826101329 Published online by Cambridge University Press

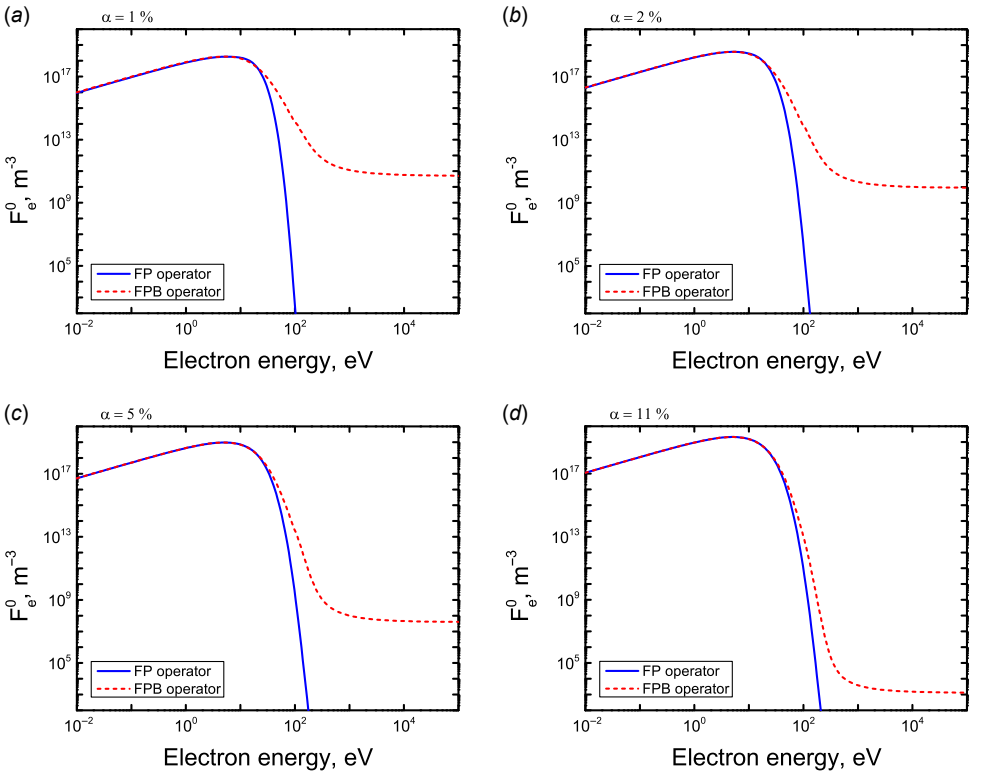


FIGURE 6. Steady-state solutions of F_e^0 with the FP (red dashed curve, $h = 0.1$) and FPB (blue solid curve, $h = 0.99$) operators. $(n_H + n_e) = 10^{18}$ m^{-3}, $T_e = 5$ eV and $E = 0.2$ Vm^{-1}. $\alpha =$ 1 %, 2 %, 5 % and 11 % for panels (*a*), (*b*), (*c*) and (*d*), respectively. (*a*) Reprinted figure with permission from Lee *et al.* (2024), copyright 2025 by the American Physical Society.

There are two exceptions that we replace: $\Delta p_{k^*} = p_{r,k^*} - p_{l,k^*}$ in (3.17) with $\Delta p_{k^*} = p_{r,k^*} - \sqrt{(E'_{1n}+1)^2 - 1}$, where k^* satisfies $T_{r,k^*} > E_{1n}$ and $T_{l,k^*} < E_{1n}$, and $\Delta p_{k^{**}} = p_{r,k^{**}} - p_{l,k^{**}}$ with $\Delta p_{k^{**}} = \sqrt{(E'_{1n}/h+1)^2 - 1} - p_{l,k^{**}}$, where k^{**} satisfies $T_{r,k^{**}} > (E_{1n})/h$ and $T_{l,k^{**}} < (E_{1n})/h$. Finally, the fully discretised form of $\mathcal{B}_{ex}^{hard}\{F_e\}$ is

$$[\mathcal{B}_{ex}^{hard}\{F_e\}(p_i,\mu_j)]_k = \sum_n \left[\frac{\Delta p_k}{\Delta p_i} \frac{\nu_{ex,1s\to np}^{hard}}{2} F_e^0(p_k) \Delta \hat{W}_{i,k}^{1n} - \nu_{ex,1s\to np}^{hard}(p_i) F_e(p_i,\mu_j) \right]. \tag{3.18}$$

4. Non-diffusive Dreicer generation in weakly ionised plasmas

In this section, we select an appropriate value of h as the ratio of the characteristic excitation energy to the critical runaway energy of interest, i.e. ∼0.1 (Lee *et al.* 2024), to account for the binary nature using the Boltzmann operator (2.23).

The non-diffusive electron acceleration mechanism that was discussed in § 2.5 is demonstrated in figure 6, where the steady-state solutions are illustrated for various ionisation fractions (corresponding to figure 5). For the demonstration,

https://doi.org/10.1017/S0022377826101329 Published online by Cambridge University Press

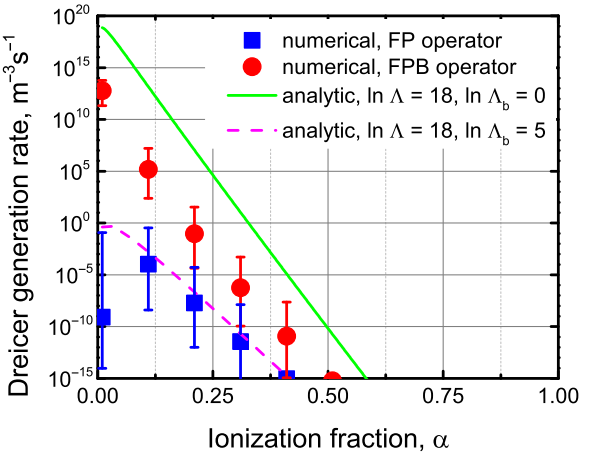


FIGURE 7. Dreicer generation rate as a function of α: with the FP (blue square, $h = 0.99$) and FPB (red circle, $h = 0.1$) operators, and the analytic formula of Connor & Hastie (1975). In the legend, ln Λ is the Coulomb logarithm for free electrons ln Λ_{free} and ln Λ_b is the logarithmic factor for bound electrons ln Λ_{bound}. For instance, ln $\Lambda_{free} = 18$ and ln $\Lambda_{bound} = 0$ for the green solid curve, and ln $\Lambda_{free} = 18$ and ln $\Lambda_{bound} = 5$ for the magenta dashed curve, required for collisional frequency computation. Here, $(n_H + n_e) = 10^{18}$ m^{-3}, $T_e = 5$ eV and $E = 0.2$ V m^{-1}. Error bars are estimated by scanning $E = 0.18$ V m^{-1} to $E = 0.22$ (± 10 %). Reprinted figure with permission from Lee *et al.* (2024), copyright 2025 by the American Physical Society.

we only took the test particle part to eliminate the runaway avalanche effect (Rosenbluth & Putvinski 1997) by setting upper boundary of integral in (2.23) to $\sqrt{(2w + b' + 2)(2w + b')}$. Blue curves in figure 6(*a–d*) represent the solutions where most collisions are described with the FP operator ($h = 0.99$). In all cases, the resulting $F_e^0 < 10^3 \mathrm{m}^{-3}$ with electron energy above 1 keV. Indeed, no Dreicer flow is expected in such conditions according to effectiveness of the Dreicer generation (Jayakumar, Fleischmann & Zweben 1993) $E/E_d^{eff} < 0.02$ with $E_d^{eff} \equiv (e^3(n_e \ln \Lambda_{free} + n_H \ln \Lambda_{bound})/4\pi\varepsilon_0^2 T_e)$, where an effect of free-bound collisions are considered by replacing $n_e \ln \Lambda_{free}$ as $n_e \ln \Lambda_{free} + n_H \ln \Lambda_{bound}$ (Martín-Solís *et al.* 2015) and $\ln \Lambda_{bound} \approx \ln \Lambda^{tot} \approx 5$ (see figure 2). The red dashed curve shows the solution with the FPB collision operator with $h = 0.1$. This solution is close to the Maxwellian in lower energy where free–free collisions dominate. However, it differs significantly at higher energy where the binary Boltzmann collisions allow for virtually free acceleration for some particles. These freely accelerated particles become runaways. The more α is, the less REs are created since continuous free–free collisions induce stronger frictions than free–bound collisions.

Figure 7 shows the Dreicer generation rate as a function of the ionisation fraction. In this case, the binary nature of collisions plays a critical role in RE generation as indicated by the condition $E/E_d > 0.025$, but $E/E_d^{eff} < 0.02$: the conventional Dreicer generation is ineffective for these parameters, while the Dreicer generation accounted by Boltzmann operator is effective and results in 10^{13} m^{-3}s^{-1} for $\alpha = 0.01$. This is consistent with the analytical indicator of effectiveness since $E/E_d \approx 0.43 \gg 0.02$, but $E/E_d^{eff} \approx 0.015$. The observed rates are much lower than the analytic prediction by Connor & Hastie (1975) without free–bound collisions

https://doi.org/10.1017/S0022377826101329 Published online by Cambridge University Press

(green curve in figure 7). Our numerical FP calculations for the Dreicer generation (blue squares) consider inelastic slowing-down and thereby agree with the Connor–Hastie formula if E_d^{eff} with $\ln \Lambda_{bound} \approx 5$ deduced from $\ln \Lambda^{tot}$ is used in the formula (dashed curve).

5. Conclusion

The collision operator for electrons in cold weakly ionised plasmas is developed to analyse the electron runaway process. The FPB operator for free–bound collisions is derived with the help of valid collision cross-sections for elastic (Itikawa 1974; Buckman & Elford 2000; Jablonski *et al.* 2004; Salvat *et al.* 2005; Breizman *et al.* 2019) and inelastic collisions (Kim & Rudd 1994; Kim *et al.* 2000; Kim 2001). The operator is invariant in particle and energy loss of electrons with respect to h since the integral boundary defining the logarithmic factor is appropriately selected (Embréus *et al.* 2018), which in turn ensures the particle and energy conservation. For free–free collisions, the validity of the linearised collision operator with sufficiently low ionisation fraction ($\sim$ middle phase of breakdown (Yoo *et al.* 2017, 2018; Yoo & Na 2022) or early burn-through (Kim *et al.* 2012)) is verified by elucidating that the Maxwell distribution function can be sustained under the strong effect of neutrals.

For numerical simulations, we present the complete analytic expression for the volume averaged form of the FPB operator. This can be implemented in the FVM-based numerical solver such as FiPy (Guyer *et al.* 2009).

Employing the FPB operator, we generalise the Dreicer generation model for weakly ionised plasmas to the non-diffusive regimes. An essential role of the binary nature of inelastic collisions is played in the Dreicer generation. Therefore, this work is envisaged to provide the precise RE generation rate for designing a runaway-free reactor start-up.

One of the promising applications of this work is to couple the kinetic model to 'fluid' plasma burn-through simulation (Kim *et al.* 2012, 2022) like fluid-kinetic disruption RE simulation (Aleynikov & Breizman 2017; Hoppe, Embreus & Fülöp 2021). This coupling will facilitate a self-consistent simulation of runaway current evolution as well as a fully kinetic description of the ionising avalanche. Moreover, the electron cyclotron pre-ionisation (Lloyd *et al.* 1991) will be investigated at a kinetic level by coupling this with nonlinear electron-cyclotron energy gain model (Suvorov & Tokman 1988; Farina & Pozzoli 1991; Farina, Pozzoli & Romé 1991; Seol, Hegna & Callen 2009; Farina 2018; Johansson & Aleynikov 2024; Gwak *et al.* 2025).

Acknowledgements

Y.L. is grateful for fruitful discussions with Dr Hyun-Tae Kim, Dr Jeongwon Lee, Professor Mathias Hoppe, Mr Jinwoo Gwak and Professor Gyungjin Choi. The views and opinions expressed herein do not necessarily reflect those of the ITER Organization.

Editor Tünde Fülöp thanks the referees for their advice in evaluating this article.

Funding

This research was supported by National R&D Program through the National Research Foundation of Korea (NRF) funded by Ministry of Science and ICT

https://doi.org/10.1017/S0022377826101329 Published online by Cambridge University Press

(2021M3F7A1084419). This research was supported by the National Research Foundation of Korea (NRF) grant funded by the Korean Government (MSIT) (RS-2024-00409564). This research was supported by R&D Program of 'Optimal Basic Design of DEMO Fusion Reactor, CN2502-1' through the Korea Institute of Fusion Energy (KFE) funded by the Government funds. The authors also gratefully acknowledge The Research Institute of Energy and Resources, The Institute of Engineering Research and the SNU Energy Initiative at Seoul National University.

Declaration of interests

The authors declare no conflicts of interest.

REFERENCES

ALEYNIKOV, P., ALEYNIKOVA, K., BREIZMAN, B., HUIJSMANS, G., KONOVALOV, S., PUTVINSKI, S. & ZHOGOLEV, V. 2014 Kinetic modelling of runaway electrons and their mitigation in ITER. In *International Atomic Energy Agency 25th Fusion Energy Conference, Saint Petersburg, Russia*, pp. 13–18.

ALEYNIKOV, P. & BREIZMAN, B.N. 2017 Generation of runaway electrons during the thermal quench in tokamaks. *Nucl. Fusion* **57**, 046009.

BELIAEV, S.T. & BUDKER, G.I. 1956 The relativistic kinetic equation. In *Soviet Physics Doklady*, vol. 1, p. 218.

BETHE, H. 1930 Zur theorie des durchgangs schneller korpuskularstrahlen durch materie. *Ann. Phys-BERLIN* **397**, 325–400.

BOHM, D. & GROSS, E.P. 1949 Theory of plasma oscillations. B. Excitation and damping of oscillations. *Phys. Rev.* **75**, 1864.

BOOZER, A.H. 2015 Theory of runaway electrons in iter: equations, important parameters, and implications for mitigation. *Phys. Plasmas* **22**, 032504.

BRAAMS, B.J. & KARNEY, C.F.F. 1987 Differential form of the collision integral for a relativistic plasma. *Phys. Rev. Lett.* **59**, 1817.

BREIZMAN, B.N., ALEYNIKOV, P., HOLLMANN, E.M. & LEHNEN, M. 2019 Physics of runaway electrons in tokamaks. *Nucl. Fusion* **59**, 083001.

BUCKMAN, S.J. & ELFORD, M.T. 2000 Momentum transfer cross sections: 2 electron collisions with atoms. In *Interactions of Photons and Electrons with Atoms*, pp. 35–55.

CHANDRASEKHAR, S. 1943 Stochastic problems in physics and astronomy. *Rev. Mod. Phys.* **15**, 1–89.

CHIU, S.C., ROSENBLUTH, M.N., HARVEY, R.W. & CHAN, V.S. 1998 Fokker–Planck simulations mylb of knock-on electron runaway avalanche and bursts in tokamaks. *Nucl. Fusion* **38**, 1711.

CONNOR, J.W. & HASTIE, R.J. 1975 Relativistic limitations on runaway electrons. *Nucl. Fusion* **15**, 415.

DREICER, H. 1959 Electron and ion runaway in a fully ionized gas. I. *Phys. Rev.* **115**, 238–249.

EMBRÉUS, O., STAHL, A. & FÜLÖP, T. 2018 On the relativistic large-angle electron collision operator for runaway avalanches in plasmas. *J. Plasma Phys.* **84**, 905840102.

FARINA, D. 2018 Nonlinear collisionless electron cyclotron interaction in the pre-ionisation stage. *Nucl. Fusion* **58**, 066012.

FARINA, D. & POZZOLI, R. 1991 Nonlinear electron-cyclotron power absorption. *Phys. Fluids B* **3**, 1570.

FARINA, D., POZZOLI, R. & ROMÉ, M. 1991 Adiabatic nonlinear interaction of a localized electron cyclotron wave with a plasma. *Phys. Fluids B* **3**, 3065.

GRIBOV, Y. *et al.* 2018 Progress in simulation of ITER first plasma operation. In *Proceedings of the 45th EPS Conference on Plasma Physics 2018 (Prague) P1.1075*.

GUREVICH, A.V. 1961 On the theory of runaway electrons. *Sov. Phys. JETP* **12**, 904–912.

GUYER, J.E., WHEELER, D. & WARREN, J.A. 2009 FiPy: partial differential equations with Python. *Comput. Sci. Eng.* **11**, 6–15.

GWAK, J., YOO, M.-G., KIM, H.-T., LEE, Y., LEE, J. & NA, Y.-S. 2025 Modelling of electron cyclotron energy gain in the tokamak pre-ionization phase. *Nucl. Fusion* **65**, 056038.

https://doi.org/10.1017/S0022377826101329 Published online by Cambridge University Press

HELANDER, P. & SIGMAR, D.J. 2005 *Collisional Transport in Magnetized Plasmas*, vol. 4. Cambridge University Press.

HESSLOW, L., EMBRÉUS, O., HOPPE, M., DUBOIS, T.C., PAPP, G., RAHM, M. & FÜLÖP, T. 2018 Generalized collision operator for fast electrons interacting with partially ionized impurities. *J. Plasma Phys.* **84**, 905840605.

HESSLOW, L., EMBRÉUS, O., STAHL, A., DUBOIS, T.C., PAPP, G., NEWTON, S.L. & FÜLÖP, T. 2017 Effect of partially screened nuclei on fast-electron dynamics. *Phys. Rev. Lett.* **118**, 255001.

HOPPE, M., EKMARK, I., BERGER, E. & FÜLÖP, T. 2022 Runaway electron generation during tokamak start-up. *J. Plasma Phys.* **88**, 905880317.

HOPPE, M., EMBREUS, O. & FÜLÖP, T. 2021 Dream: a fluid-kinetic framework for tokamak disruption runaway electron simulations. *Comput. Phys. Commun.* **268**, 108098.

INOKUTI, M. 1971 Inelastic collisions of fast charged particles with atoms and molecules – the bethe theory revisited. *Rev. Mod. Phys.* **43**, 297.

ITIKAWA, Y. 1974 Momentum-transfer cross sections for electron collisions with atoms and molecules. *Atom. Data Nucl. Data* **14**, 1–10.

JABLONSKI, A., SALVAT, F. & POWELL, C.J. 2004 Comparison of electron elastic-scattering cross sections calculated from two commonly used atomic potentials. *J. Phys. Chem. Ref. Data* **33**, 409–451.

JAYAKUMAR, R., FLEISCHMANN, H.H. & ZWEBEN, S.J. 1993 Collisional avalanche exponentiation of runaway electrons in electrified plasmas. *Phys. Lett. A* **172**, 447–451.

JOHANSSON, C.A. & ALEYNIKOV, P. 2024 Electron cyclotron resonance during plasma initiation. *J. Plasma Phys.* **90**, 905900103.

KIM, H.-T. *et al.* 2022 Development of full electromagnetic plasma burn-through model and validation in MAST. *Nucl. Fusion* **62**, 126012.

KIM, H.-T. & Fundamenski, Wojciech, Sips, ACC & Contributors 2012 Enhancement of plasma burn-through simulation and validation in JET. *Nucl. Fusion* **52**, 103016.

KIM, Y.-K. 2001 Scaling of plane-wave born cross sections for electron-impact excitation of neutral atoms. *Phys. Rev. A* **64**, 032713.

KIM, Y.-K. & RUDD, M.E. 1994 Binary-encounter-dipole model for electron-impact ionization. *Phys. Rev. A* **50**, 3954–3967.

KIM, Y.-K., SANTOS, J.P. & PARENTE, F. 2000 Extension of the binary-encounter-dipole model to relativistic incident electrons. *Phys. Rev. A* **62**, 052710.

KIRILLOV, V.D., TRUBNIKOV, B.A. & TRUSHIN, S.A. 1975 Role of impurities in anomalous plasma resistance. *Sov. J. Plasma Phys.(Engl. Transl.); (USA)* **1**.

KNOEPFEL, H. & SPONG, D.A. 1979 Runaway electrons in toroidal discharges. *Nucl. Fusion* **19**, 785.

KNOEPFEL, H. & ZWEBEN, S.J. 1975 High-energy runaway electrons in the oak ridge tokamak. *Phys. Rev. Lett.* **35**, 1340–1343.

LANDAU, L.D., LIFSHITZ, E.M. & PITAEVSKIJ, L.P. 1981 *Course of Theoretical Physics*, Physical Kinetics, vol. 10. Pergamon Press.

LANDAU, L.D. & LIFSHITZ, E.M. 2013 *Quantum Mechanics: Non-Relativistic Theory*, vol. 3. Elsevier.

LEE, J. *et al.* 2023*a* Validation of a plasma burn-through simulation with an ech power absorption model in kstar. *Phys. Scr.* **98**, 055610.

LEE, Y. *et al.* 2023*b* Kinetic modelling of start-up runaway electrons in kstar and iter. *Nucl. Fusion* **63**, 106011.

LEE, Y., ALEYNIKOV, P., DE VRIES, P.C., KIM, H.-T., LEE, J., HOPPE, M., PARK, J.-K., CHOI, G.J., GWAK, J. & NA, Y.-S. 2024 Binary nature of collisions facilitates runaway electron generation in weakly ionized plasmas. *Phys. Rev. Lett.* **133**, 175102.

LEHNEN, M., BOZHENKOV, S.A., ABDULLAEV, S.S. & JAKUBOWSKI, M.W. 2008 Suppression of runaway electrons by resonant magnetic perturbations in textor disruptions. *Phys. Rev. Lett.* **100**, 255003.

LI, B. & ERNST, D.R. 2011 Gyrokinetic fokker–Planck collision operator. *Phys. Rev. Lett.* **106**, 195002.

LIU, C., LVOVSKIY, A., PAZ-SOLDAN, C., JARDIN, S.C. & BHATTACHARJEE, A. 2023 Self-consistent simulation of the excitation of compressional alfvén eigenmodes and runaway electron diffusion in tokamak disruptions. *Phys. Rev. Lett.* **131**, 085102.

https://doi.org/10.1017/S0022377826101329 Published online by Cambridge University Press

LLOYD, B., JACKSON, G.L., TAYLOR, T.S., LAZARUS, E.A., LUCE, T.C. & PRATER, R. 1991 Low voltage ohmic and electron cyclotron heating assisted startup in diii-d. *Nucl. Fusion* **31**, 2031.

MARTÍN-SOLÍS, J.R., LOARTE, A. & LEHNEN, M. 2015 Runaway electron dynamics in tokamak plasmas with high impurity content. *Phys. Plasmas* **22**, 092512.

MARTÍN-SOLÍS, J.R., LOARTE, A. & LEHNEN, M. 2017 Formation and termination of runaway beams in iter disruptions. *Nucl. Fusion* **57**, 066025.

MATSUYAMA, A., WAKATSUKI, T., INOUE, S., YAMAMOTO, Y., YOSHIDA, M. & URANO, H. 2022 Modelling of ohmic startup and runaway electron formation in support of jt-60sa initial operation. *Nucl. Fusion* **63**, 026001.

MATTHEWS, G.F. *et al.* 2016 Melt damage to the jet iter-like wall and divertor. *Phys. Scr.* **2016**, 014070.

MCDEVITT, C.J., GUO, Z. & TANG, X.-Z. 2019 Avalanche mechanism for runaway electron amplification in a tokamak plasma. *Plasma Phys. Control. Fusion* **61**, 054008.

MØLLER, C. 1932 Zur theorie des durchgangs schneller elektronen durch materie. *Ann. Phys-BERLIN* **406**, 531–585.

MOSHER, D. 1975 Interactions of relativistic electron beams with high atomic-number plasmas. *Phys. Fluids* **18**, 846–857.

MOTT, N.F. 1930 The collision between two electrons. *Proc. R. Soc. Lond. Ser. A, Contain. Pap. Math. Phys. Charact.* **126**, 259–267.

NYGREN, R., LUTZ, T., WALSH, D., MARTIN, G., CHATELIER, M., LOARER, T. & GUILHEM, D. 1997 Runaway electron damage to the tore supra phase III outboard pump limiter. *J. Nucl. Mater.* **241–243**, 522–527.

PAPP, G., DREVLAK, M., FÜLÖP, T. & HELANDER, P. 2011 Runaway electron Drift orbits in magnetostatic perturbed fields. *Nucl. Fusion* **51**, 043004.

REUX, C. 2021 Demonstration of safe termination of megaampere relativistic electron beams in tokamaks. *Phys. Rev. Lett.* **126**, 175001.

RICHARDSON, A.S. 2019 NRL plasma formulary. *Tech. Rep.* US Naval Research Laboratory.

ROSENBLUTH, M.N. & PUTVINSKI, S.V. 1997 Theory for avalanche of runaway electrons in tokamaks. *Nucl. Fusion* **37**, 1355.

ROSENBLUTH, M.N., MACDONALD, W.M. & JUDD, D.L. 1957 Fokker–Planck equation for an inverse-square force. *Phys. Rev.* **107**, 1–6.

SALVAT, F., JABLONSKI, A. & POWELL, C.J. 2005 Elsepa–Dirac partial-wave calculation of elastic scattering of electrons and positrons by atoms, positive ions and molecules. *Comput. Phys. Commun.* **165**, 157–190.

SANDQUIST, P., SHARAPOV, S.E., HELANDER, P. & LISAK, M. 2006 Relativistic electron distribution function of a plasma in a near-critical electric field. *Phys. Plasmas* **13**, 072108.

SAVOYE-PEYSSON, Y., MAZON, D., BIELECKI, J., DWORAK, D., KRÓL, K., JARDIN, A., SCHOLZ, M., WALKOWIAK, J. & DECKER, J. 2023 A unified description of atomic physics for electron Fokker–Planck calculations. *Nucl. Fusion* **63**, 126041.

SEOL, J.C., HEGNA, C.C. & CALLEN, J.D. 2009 Nonlinear cyclotron harmonic absorption. *Phys. Plasmas* **16**, 052512.

SHARMA, A.S. & JAYAKUMAR, R. 1988 Runaway electrons during tokamak startup. *Nucl. Fusion* **28**, 491.

SNIPES, J.A., PARKER, R.R., PHILLIPS, P.E., SCHMIDT, A. & WALLACE, G. 2008 Fast electron driven Alfvén eigenmodes in the current rise in alcator c-mod. *Nucl. Fusion* **48**, 072001.

SOLODOV, A.A. & BETTI, R. 2008 Stopping power and range of energetic electrons in dense plasmas of fast-ignition fusion targets. *Phys. Plasmas* **15**, 042707.

STONE, P.M., KIM, Y.-K. & DESCLAUX, J.P. 2002 Electron-impact cross sections for dipole-and spin-allowed excitations of hydrogen, helium, and lithium. *J. Res. Natl. Inst. Stan.* **107**, 327.

SUVOROV, E.V. & TOKMAN, M.D. 1988 Generation of accelerated electrons during cyclotron heating of plasmas. *Sov. J. Plasma Phys. (Engl. Transl.); (USA)* **14**.

DE VRIES, P.C. & GRIBOV, Y. 2019 Iter breakdown and plasma initiation revisited. *Nucl. Fusion* **59**, 096043.

DE VRIES, P.C., GRIBOV, Y., MARTIN-SOLIS, R., MINEEV, A.B., SINHA, J., SIPS, A.C.C., KIPTILY, V., LOARTE, A. & Contributors JET 2020 Analysis of runaway electron discharge formation during joint european torus plasma start-up. *Plasma Phys. Control. Fusion* **62**, 125014.

https://doi.org/10.1017/S0022377826101329 Published online by Cambridge University Press

DE VRIES, P.C. *et al.* 2023 Cross-machine comparison of runaway electron generation during tokamak start-up for extrapolation to iter. *Nucl. Fusion* **63**, 086016.

DE VRIES, P.C. 2025 Comparison of start-up runaway electron generation simulations using the scenplint code with jet experimental observations. *Nucl. Fusion* **65**, 056001.

WALKOWIAK, J., JARDIN, A., BIELECKI, J., PEYSSON, Y., MAZON, D., DWORAK, D., KRÓL, K. & SCHOLZ, M. 2022 Approximate atomic models for fast computation of the Fokker–Planck equation in fusion plasmas with high-z impurities and suprathermal electrons. *Phys. Plasmas* **29**, 022501.

WILSON, C.T.R. 1925 The acceleration of β-particles in strong electric fields such as those of thunderclouds. *Math. Proc. Camb.* **22**, 534–538.

YOO, M.-G. *et al.* 2018 Evidence of a turbulent exb mixing avalanche mechanism of gas breakdown in strongly magnetized systems. *Nat. Commun.* **9**, 3523.

YOO, M.-G., LEE, J., KIM, Y.-G. & NA, Y.-S. 2017 Development of 2d implicit particle simulation code for ohmic breakdown physics in a tokamak. *Comput. Phys. Commun.* **221**, 143–159.

YOO, M.-G. & NA, Y.-S. 2022 Understanding the electromagnetic topology during the ohmic breakdown in tokamaks considering self-generated electric fields. *Plasma Phys. Control. Fusion* **64**, 054008.

ZHOGOLEV, V. & KONOVALOV, S. 2014 Characteristics of interaction of energetic electrons with heavy impurity ions in a tokamak plasma. *VANT Prob. Atom. Sci. Tech. Ser. Thermonucl. Fusion* **37**, 71.

https://doi.org/10.1017/S0022377826101329 Published online by Cambridge University Press